NASA Tech Briefs

National Aeronautics and Space Administration

Electronic Components and Circuits

Electronic Systems

Physical Sciences

Materials

Computer Programs

Mechanics

Machinery

Fabrication Technology

Mathematics and Information Sciences

Life Sciences

INTRODUCTION

Tech Briefs are short announcements of innovations originating from research and development activities of the National Aeronautics and Space Administration. They emphasize information considered likely to be transferable across industrial, regional, or disciplinary lines and are issued to encourage commercial application.

Availability of NASA Tech Briefs and TSPs

Requests for individual Tech Briefs or for Technical Support Packages (TSPs) announced herein should be addressed to

National Technology Transfer Center
Telephone No. **(800) 678-6882** or via World Wide Web at **www2.nttc.edu/leads/**

Please reference the control numbers appearing at the end of each Tech Brief. Information on NASA's Commercial Technology Team, its documents, and services is also available at the same facility or on the World Wide Web at **www.nctn.hq.nasa.gov**.

Commercial Technology Offices and Patent Counsels are located at NASA field centers to provide technology-transfer access to industrial users. Inquiries can be made by contacting NASA field centers and program offices listed below.

NASA Field Centers and Program Offices

Ames Research Center
Carolina Blake
(650) 604-1754 or
cblake@mail.arc.nasa.gov

Dryden Flight Research Center
Jenny Baer-Riedhart
(661) 276-3689 or
jenny.baer-riedhart@dfrc.nasa.gov

Goddard Space Flight Center
George Alcorn
(301) 286-5810 or
galcorn@gsfc.nasa.gov

Jet Propulsion Laboratory
Merle McKenzie
(818) 354-2577 or
merle.mckenzie@jpl.nasa.gov

Johnson Space Center
Hank Davis
(281) 483-0474 or
henry.l.davis1@jsc.nasa.gov

John F. Kennedy Space Center
Jim Aliberti
(321) 867-6224 or
Jim.Aliberti-1@ksc.nasa.gov

Langley Research Center
Sam Morello
(757) 864-6005 or
s.a.morello@larc.nasa.gov

Glenn Research Center
Larry Viterna
(216) 433-3484 or
cto@grc.nasa.gov

George C. Marshall Space Flight Center
Vernotto C. McMillan
(256) 544-2615 or
vernotto.mcmillan@msfc.nasa.gov

John C. Stennis Space Center
Kirk Sharp
(228) 688-1929 or
technology@ssc.nasa.gov

NASA Program Offices
At NASA Headquarters there are seven major program offices that develop and oversee technology projects of potential interest to industry:

Carl Ray
Small Business Innovation Research Program (SBIR) & Small Business Technology Transfer Program (STTR)
(202) 358-4652 or
cray@mail.hq.nasa.gov

Dr. Robert Norwood
Office of Commercial Technology (Code RW)
(202) 358-2320 or
rnorwood@mail.hq.nasa.gov

John Mankins
Office of Space Flight (Code MP)
(202) 358-4659 or
jmankins@mail.hq.nasa.gov

Terry Hertz
Office of Aero-Space Technology (Code RS)
(202) 358-4636 or
thertz@mail.hq.nasa.gov

Glen Mucklow
Office of Space Sciences (Code SM)
(202) 358-2235 or
gmucklow@mail.hq.nasa.gov

Roger Crouch
Office of Microgravity Science Applications (Code U)
(202) 358-0689 or
rcrouch@hq.nasa.gov

Granville Paules
Office of Mission to Planet Earth (Code Y)
(202) 358-0706 or
gpaules@mtpe.hq.nasa.gov

BLANK PAGE

NASA TechBriefs

National Aeronautics and Space Administration

February 2002
02-02

BLANK PAGE

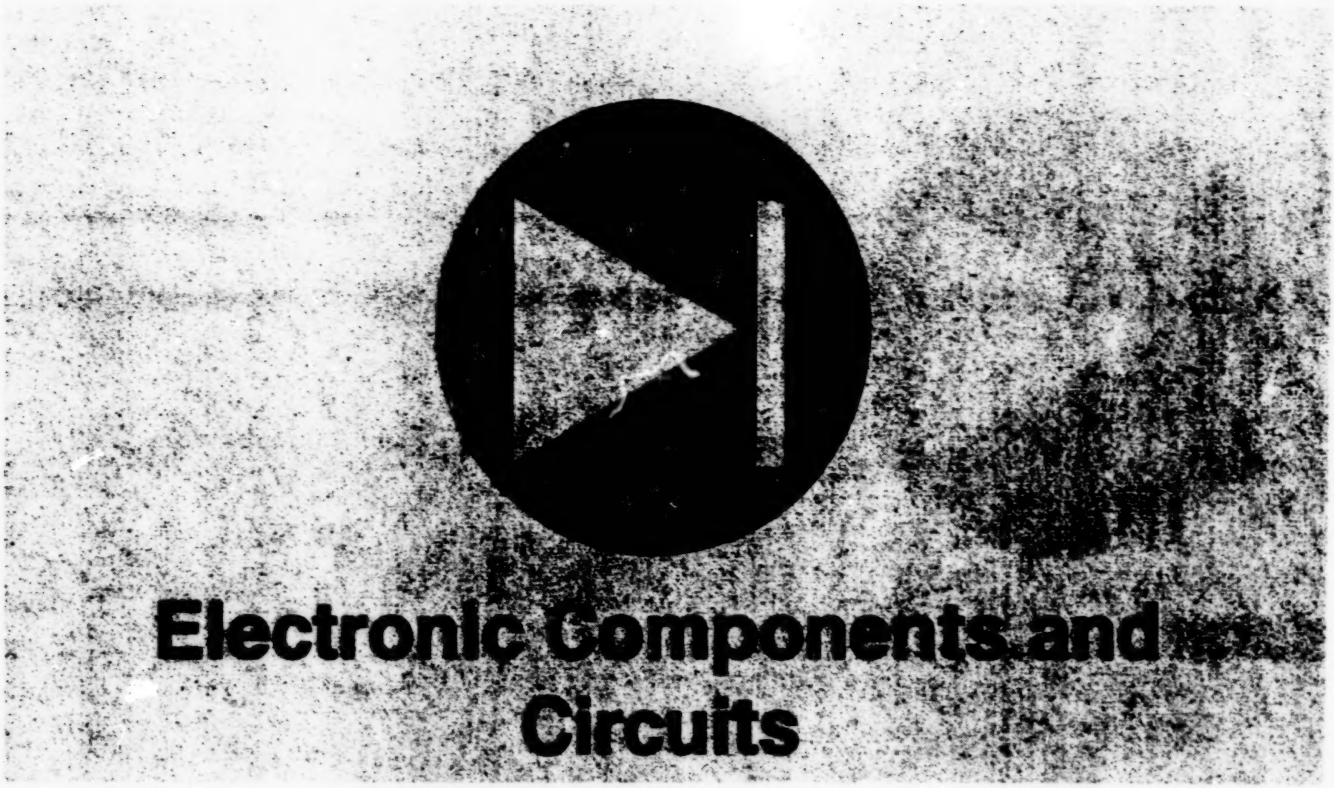

Electronic Components and Circuits

Hardware, Techniques, and Processes

BLANK PAGE

InP HEMT MMIC Low-Noise Amplifier for 65 to 110 GHz

Copies performed substantially as designed in cryogenic and room-temperature tests.

NASA's Jet Propulsion Laboratory, Pasadena, California

MODULE CONTAINING AMPLIFIER

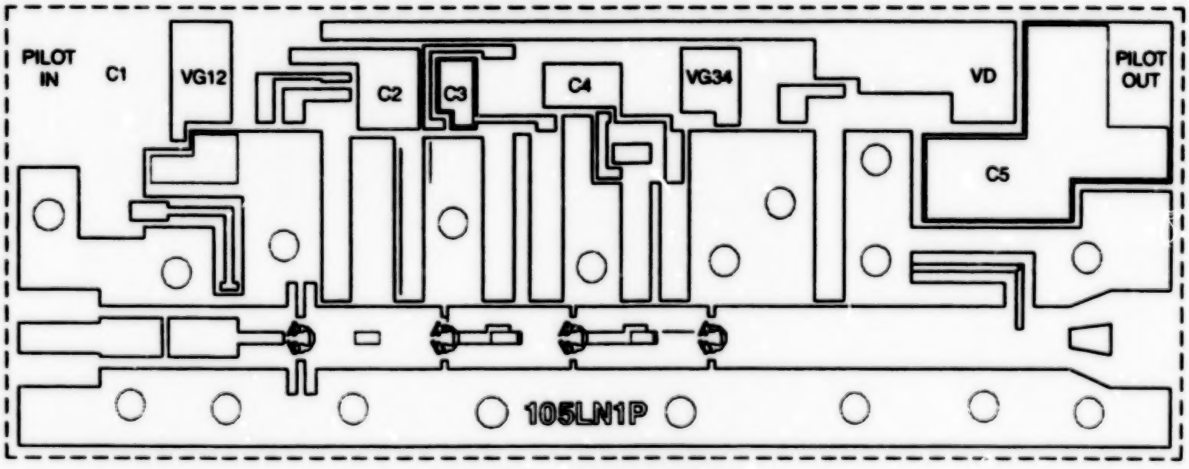

MAGNIFIED LAYOUT OF AMPLIFIER

A Four-Stage MMIC LNA is mounted in a split-block waveguide module. The dimensions of the MMIC chip are 2 by 0.73 by 0.075 mm.

A monolithic microwave integrated circuit (MMIC) has been designed to function as a low-power-consumption, low-noise amplifier (LNA) at frequencies from about 65 to about 110 GHz. This MMIC incorporates TRW's state-of-the-art, InP-based, high-electron-mobility transistors (HEMTs) coupled with coplanar-waveguide (CPW) transmission lines, thin-film resistors, and thin-film capacitors. The MMIC is mounted in a waveguide module with CPW-to-waveguide transitions of the probe type (see figure).

An unusual feature of the circuit is a path for a pilot signal with a typical frequency of 500 MHz. This path is through the same transistors used to amplify the millimeter-wave signal. The pilot signal is applied through a pilot input terminal (the upper left pad in the figure) and appears at a pilot output terminal (the upper right pad in the figure). The low-level pilot signal is coupled from one bias circuit to the next and does not interact appreciably with the millimeter-wave signal. The pilot signal is meant to be used to measure fluctuations in the gain of the transistors; such measurements are useful in applications (e.g., radiometry) in which fluctuations in gain can affect measurements.

The MMIC is designed to operate in the presence of cooling by a suitable cryogenic apparatus. Seventeen waveguide modules containing copies of the MMIC were tested for noise temperature by use of a variable-temperature waveguide with a 20-dB attenuator and a precise diode temperature sensor. The range of noise temperatures over the 85-to-115-GHz frequency range was found to be 30 to 107 K at an operating temperature of 24 K. The noise at room operating temperature was found to range from 250 to 470 K. In other tests, the MMICs were found to be capable of producing 20 dB of gain while consuming as little as 1.4 mW of dc power.

This work was done by Todd Gaier and Sander Weinreb of Caltech, Neal Erickson of the University of Massachusetts, and Richard Lai of TRW for **NASA's Jet Propulsion Laboratory**. *Further information is contained in a TSP [see page 1].*

NPO-20752

"Substrateless" Millimeter- and Submillimeter-Wave Circuits

Radio-frequency losses are reduced by suspending conductors in air.

NASA's Jet Propulsion Laboratory, Pasadena, California

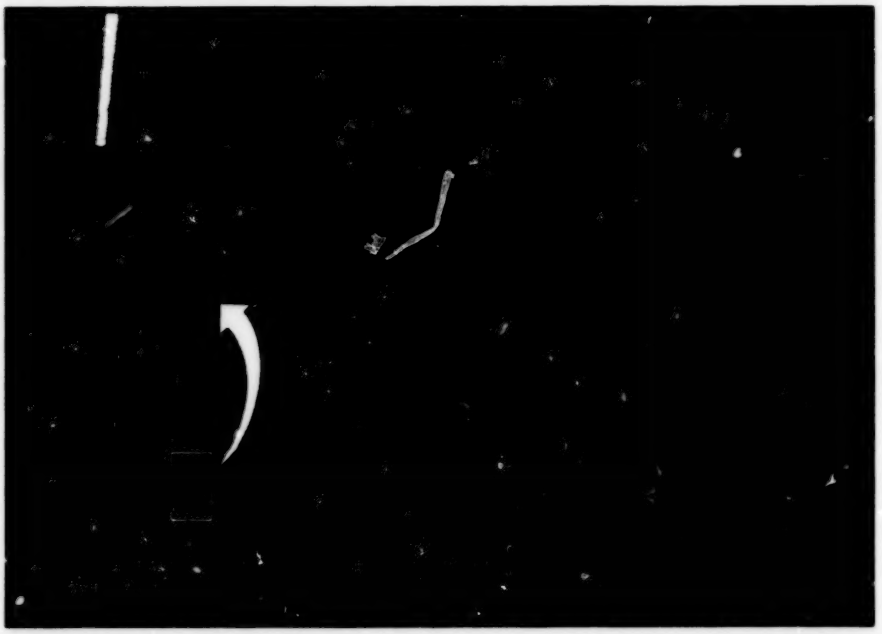

A "Substrateless" 400-GHz Frequency Doubler is mounted in a crossed-waveguide block for testing.

Monolithic integrated circuits (in particular, Schottky-diode-based frequency multipliers) that operate at frequencies as high as a few terahertz are being developed in a program that utilizes the recent advances in methods of computer-aided design and microfabrication. In the approach followed in this program, the active semiconductor devices (GaAs-based Schottky diodes) in a frequency-multiplier circuit are integrated with passive devices (planar metal transmission lines). To reduce radio-frequency losses associated with dielectric layers in the passive circuitry, the semiconductor substrate under the transmission lines is etched away, leaving metal conductors insulated by air and held only by their edges on a semiconductor frame. The monolithic integration makes the integrated circuit larger (in comparison with discrete circuit components that one would otherwise have to assemble), thereby making the circuit more robust and easier to handle in fabrication and mounting. Metallic beam-leads are used extensively, serving as (1) mechanical handles that facilitate handling and mounting, (2) current paths for dc grounding and biasing of the diodes, and (3) thermal conductors. Moreover, this approach enables the precise positioning of the diodes with respect to the rest of the circuitry and facilitates scaling for operation at higher frequencies.

Following this approach, a frequency multiplier is designed in a three-stage process. In the first stage, one uses (1) a computer program that simulates nonlinear circuits and (2) a computer program that implements a mathematical model of a diode in conjunction with a harmonic-balance-based simulator computer program to optimize the dimensions, doping profile, and number of diodes to be used in the circuit. This stage yields the diode-junction characteristics and embedding impedances that give the best performance.

In the second stage, the input and output impedance-matching transmission line circuits are designed by use of finite-element electromagnetic-simulator software. The numerical output of this software comprises scattering-parameter matrices referenced to diode and transmission-line ports. The matrices plus the embedding impedances computed by the nonlinear-circuit simulator software are then provided as input to linear-circuit simulator software, which is used to analyze the impedance-matching effectiveness of the input and output transmission-line circuits. The parasitics associated with the diode(s) are included in this analysis as part of the passive circuit.

To simplify and speed up the analysis, the passive circuitry is divided into small elements at electromagnetically appropriate points, giving rise to several S-parameter matrices. Ports are modeled as being attached to probes on each anode so that the individual embedding impedance for each diode can be calculated directly. The diodes are then modeled as being embedded into the resulting cascaded S-parameter matrix blocks to determine the total efficiency and the power performance of the multiplier. If these are unsatisfactory, relative to the intrinsic efficiency and performance of the diodes, the circuit design is iteratively modified to correct for the parasitics found in the simulation.

Standard processing techniques, including stepper lithography and reactive-ion etching, are used to fabricate the diode structures on the front side of a GaAs wafer. The diodes are located on an edge of that portion of the GaAs wafer that is destined to remain as a transmission-line-supporting frame. After front-side processing has been completed, a back-side procedure is used to remove the GaAs under the metal conductors of the input and output transmission lines, except for edge supports as described above.

Thus far, two types of frequency-doubler circuits, designed for output frequencies of 200 and 400 GHz, respectively, have been designed, fabricated, and tested (see figure). Notwithstanding a need for further iteration to optimize design, the results of the tests are encouraging: For example, in a test in which the input frequency ranged from 179 to 212 GHz, one of the 400-GHz units exhibited a peak efficiency and peak power of ≈15 percent and ≈6 mW, respectively, at an output frequency of 369 GHz at room temperature. This represents a new performance record from planar Schottky diode varactors at this frequency.

This work was done by Imran Mehdi, Suzanne Martin, Jean Bruston, Erich Schlecht, and R. P. Smith of Caltech for **NASA's Jet Propulsion Laboratory**. *Further information is contained in a TSP [see page 1].*

In accordance with Public Law 96-517, the contractor has elected to retain title to this invention. Inquiries concerning rights for its commercial use should be addressed to

Technology Reporting Office
JPL
Mail Stop 249-103
4800 Oak Grove Drive
Pasadena, CA 91109
(818) 354-2240

Refer to NPO-21080, volume and number of this NASA Tech Briefs *issue, and the page number.*

Unity-Power-Factor Interfaces for Data-Processing Equipment

These could be manufactured as plug-in units.

John F. Kennedy Space Center, Florida

Circuits for conditioning AC power supplied to computers are under development. A power conditioner of this type would be an interface between a conventional AC power line and a computer power supply (that is, an AC-to-DC converter) that contains one or more rectifier(s) and inductor(s). Typically, such a power converter is characterized by a power factor <1, and, because it presents a nonlinear load to the power line, it injects currents at harmonics of the power-line frequency back into the power line. These harmonic currents can cause interference with the operations of other electronic equipment as well as overheating of power-line transformers.

The main purpose served by the power conditioner is to prevent injection of the harmonics into the power line and to bring the power factor up to 1. It would not be necessary to modify either the computer power supply or the AC-power-distribution system. Instead, the power conditioner could be manufactured as a plug-in unit that could simply be inserted between an AC outlet and the computer AC-power plug. Hence, it would be easy to retrofit a previously constructed system with power conditioners.

The effects of power factors <1 and power-line harmonics on power-distribution systems and data-processing equipment are well known. Prior to the present development, efforts to suppress these effects had included the development of unity-power-factor (UPF) rectifiers that include active current-shaping circuits to make the power-line currents drawn by the rectifiers sinusoidal. However, such rectifiers have not become popular in commercial data-processing equipment.

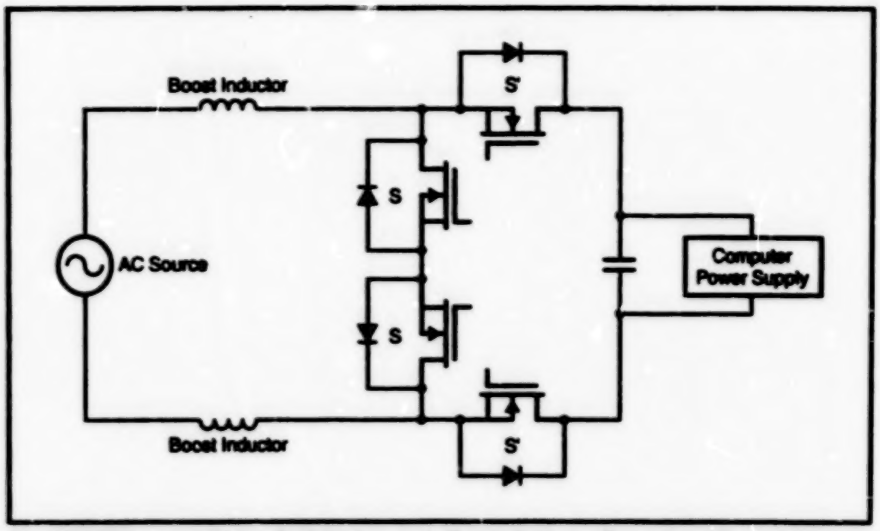

The MOSFETs S and S′ Are Switched on and off periodically to effect pulse-width modulation to shape the source current to a purely sinusoidal waveform when presented with a nonlinear load like a computer power supply.

The present developmental power conditioners can be characterized as boost AC-to-AC converters. Like the UPF rectifiers, these power converters utilize current shaping. In particular, they utilize pulse-width modulation as a versatile means of shaping currents to control the flow of power. The modulation in such a power converter is controlled by a combination of an inner average-current loop and an outer voltage-control loop. Together, these control loops maintain a regulated output voltage while forcing the input current to be sinusoidal.

The figure is a simplified schematic diagram of such a power conditioner for a single-phase power line. When the metal oxide semiconductor field-effect transistors (MOSFETs) labeled S are turned on, the magnitude of source current through the boost inductors increases. When the MOSFETs labeled S′ are turned on, the magnitude of the current through the boost inductors decreases. Hence, by suitably modulating the switching of S and S′, the source current can be controlled to be sinusoidal.

This work was done by David Loftus of GSE Technology Applications and Giri Venkataramanan of Montana State University for **Kennedy Space Center.** *Further information is contained in a TSP [see page 1].*

KSC-12147

Mixed-Signal Driver ASIC for IEEE 1394 and I²C Buses

Radiation-hardened ASICs enable communication among three different buses.

NASA's Jet Propulsion Laboratory, Pasadena, California

The IEEE 1394 and I²C Mixed-Signal Driver is one of two application-specific integrated circuits (ASICs) designed to function together as an interface among the following three digital-signal buses:

- A peripheral component interface (PCI) bus;
- A high-speed serial data bus that conforms to Institute of Electrical and Electronics Engineers (IEEE) standard 1394, also known as the FireWire standard; and
- An I²C (inter integrated circuit) bus, which was developed in the early 1980s by Philips Semiconductors for connecting a central processing unit to peripheral integrated-circuit chips in a television receiver.

Among other things that have been emphasized in the development effort are radiation hardness and compactness as required for intended use aboard spacecraft. As result of engineering compromises necessary for radiation hardness, the performance of this set of ASICs is expected to lag somewhat behind that of comparable circuitry previously developed for terrestrial use. Nevertheless, because the capability for communication among the three buses is not afforded by any plug-in circuit cards now commercially available, there could be a terrestrial market for these ASICs for applications in which the tri-bus communication is required.

In the original spacecraft application, the two ASICs would enable communication among multiple computers, scientific instruments, and spacecraft engineering systems via the three buses. The first ASIC, which could be characterized as a digital input/output (DIO) ASIC, would provide a digital interface (a link layer) among the three buses. The second ASIC, denoted the IEEE 1394 and I²C Mixed-Signal Input/Output Driver ASIC ("MSIO ASIC" for short) is the focus of this article. The MSIO ASIC would serve as the physical layer in the overall data-communication architecture.

The MSIO ASIC would implement an analog interface to the IEEE 1394 and I²C bus cables. The MSIO ASIC would be connected, either directly or through an isolation transformer, to the DIO ASIC. The MSIO ASIC would receive digital commands and data from the DIO ASIC and pass these data and commands out through the IEEE 1394 and I²C cables. The MSIO would contain a commercial controller core, custom analog bus cable-driver circuits, two I²C-bus cable-driver cores, and custom glue-logic circuitry. The MSIO ASIC would be a radiation-hardened, galvanically isolated, three-port implementation of the physical-layer functions described in the IEEE 1394a D2.0 draft specification. The MSIO ASIC would also contain two radiation-hardened, galvanically isolated sets of I²C drivers and receivers, independent of the 1394 interface and of each other.

This work was done by Huy Long, Peter Jones, Savio Chau, and Eric Holmberg of Caltech and Ross McTaggert of Digital MediaCom for **NASA's Jet Propulsion Laboratory**. *Further information is contained in a TSP [see page 1].*

In accordance with Public Law 96-517, the contractor has elected to retain title to this invention. Inquiries concerning rights for its commercial use should be addressed to

Intellectual Property group
JPL
Mail Stop 202-233
4800 Oak Grove Drive
Pasadena, CA 91109
(818) 354-2240

Refer to NPO-30121, volume and number of this NASA Tech Briefs *issue, and the page number.*

Optoelectronic Oscillator With Low Acceleration Sensitivity

A fiber-optic delay line is arranged to minimize changes in optical-path length.

NASA's Jet Propulsion Laboratory, Pasadena, California

An optoelectronic oscillator with a nominal operating frequency of 11.763 GHz has been designed and constructed to demonstrate a technique for reducing the sensitivity of the operating frequency to acceleration. Optoelectronic oscillators in general exhibit low sensitivity to acceleration in addition to other attractive characteristics (high spectral purity, low phase noise, capability for generating multigigahertz frequencies, and both electrical and optical input and output capabilities). The practical significance of the present development is that the reduction of acceleration sensitivities to exceptionally low levels would render optoelectronic oscillators even more attractive as signal sources for use on diverse moving platforms, including automobiles, ships, aircraft, and spacecraft.

The optoelectronic oscillator (see Figure 1) includes a distributed-feedback laser and a feedback loop that comprises a semiconductor Mach-Zehnder electro-optical modulator, a delay line that consists of a coiled 2-km-long optical fiber, a photodetector, a microwave amplifier, and a band-pass filter. The oscillator also includes an electronic controller that drives the laser, regulates the temperature of the laser, biases the modulator and the photodetector, and supplies power to the microwave amplifier. All of the oscillator components except the fiber-optic delay line are packaged in a module that amounts to a prototype of "turn-key" (fully operational) optoelectronic oscillator units.

Of course, firm mounting of the components within the module is an essential part of the design for reducing sensitivity to acceleration. Most of the remaining sensitivity to acceleration is attributable to accel-

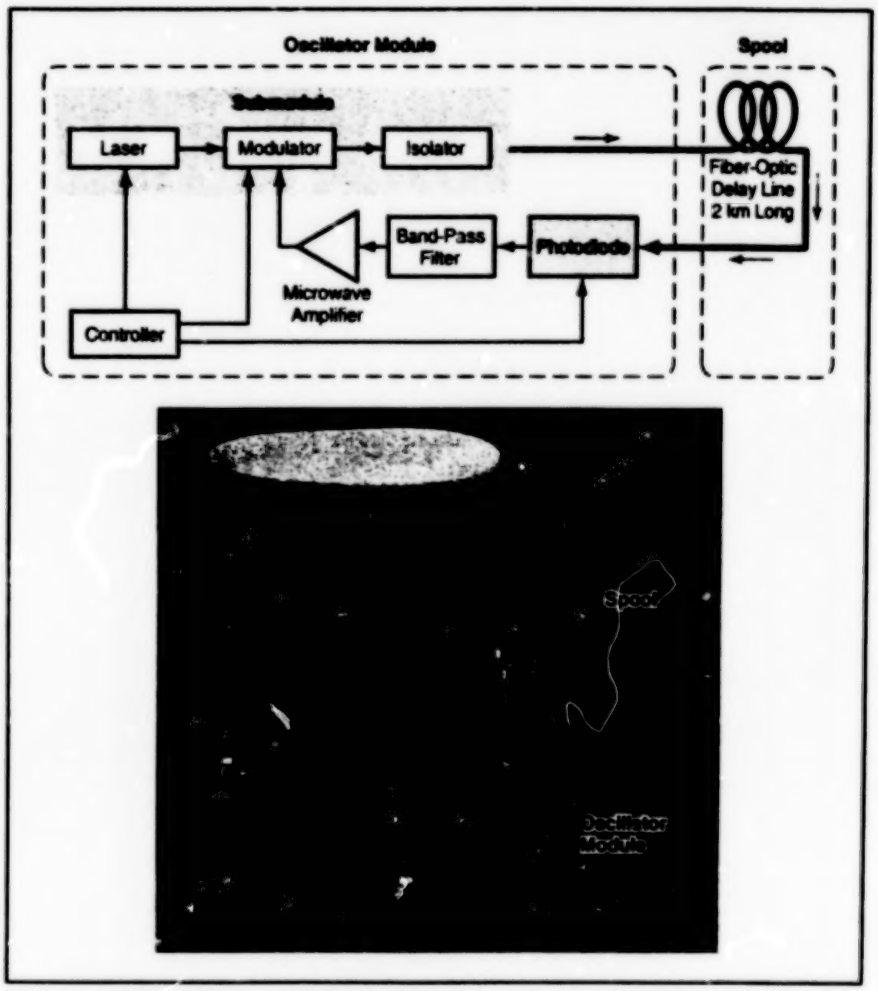

Figure 1. The Optoelectronic Oscillator (shown here before modification to reduce sensitivity to acceleration) comprises an oscillator module and a fiber-optic delay line.

eration-induced changes in the length of the optical path along the fiber-optic delay line; therefore, the problem of desensitization to acceleration becomes one of minimizing these changes.

Experiments and calculations have shown that if the fiber-optic delay line is coiled tightly on a spool, then the sensitivity to acceleration perpendicular to the spool axis is less than 1/20 of the sensitivity to acceleration along the spool axis. Hence, the problem is reduced further in that it should be possible to eliminate most of the sensitivity to acceleration by concentrating on minimizing the response to acceleration along the spool axis.

The solution of the problem is to split the fiber-optic delay line into two coils that are of opposite chirality but are otherwise identical and that are mounted on opposite faces of the oscillator module (see Figure 2). In principle, when acceleration along the spool axis lengthens the optical path in one coil by a given amount, it should shorten the optical path in the other coil by the same amount, so that the net change in optical-path length should be zero. Measurements have shown that the sensitivity is reduced to about 1/40 of that obtained of a single-coil version of the delay line. The total sensitivity to acceleration along all three axes was found to be less than 1.5×10^{-10} g^{-1} ($\approx 1.5 \times 10^{-11}$ s^2/m), where g (≈ 9.8 m/s^2) is the gravitational acceleration at the surface of the Earth.

This work was done by Shouhua Huang, Meirong Tu, and X. Steve Yao of Caltech for **NASA's Jet Propulsion Laboratory.** *Further information is contained in a TSP [see page 1].*

In accordance with Public Law 96-517, the contractor has elected to retain title to this invention. Inquiries concerning rights for its commercial use should be addressed to

Technology Reporting Office
JPL
Mail Stop 249-103
4800 Oak Grove Drive
Pasadena, CA 91109
(818) 354-2240

Refer to NPO-21003, volume and number of this NASA Tech Briefs *issue, and the page number.*

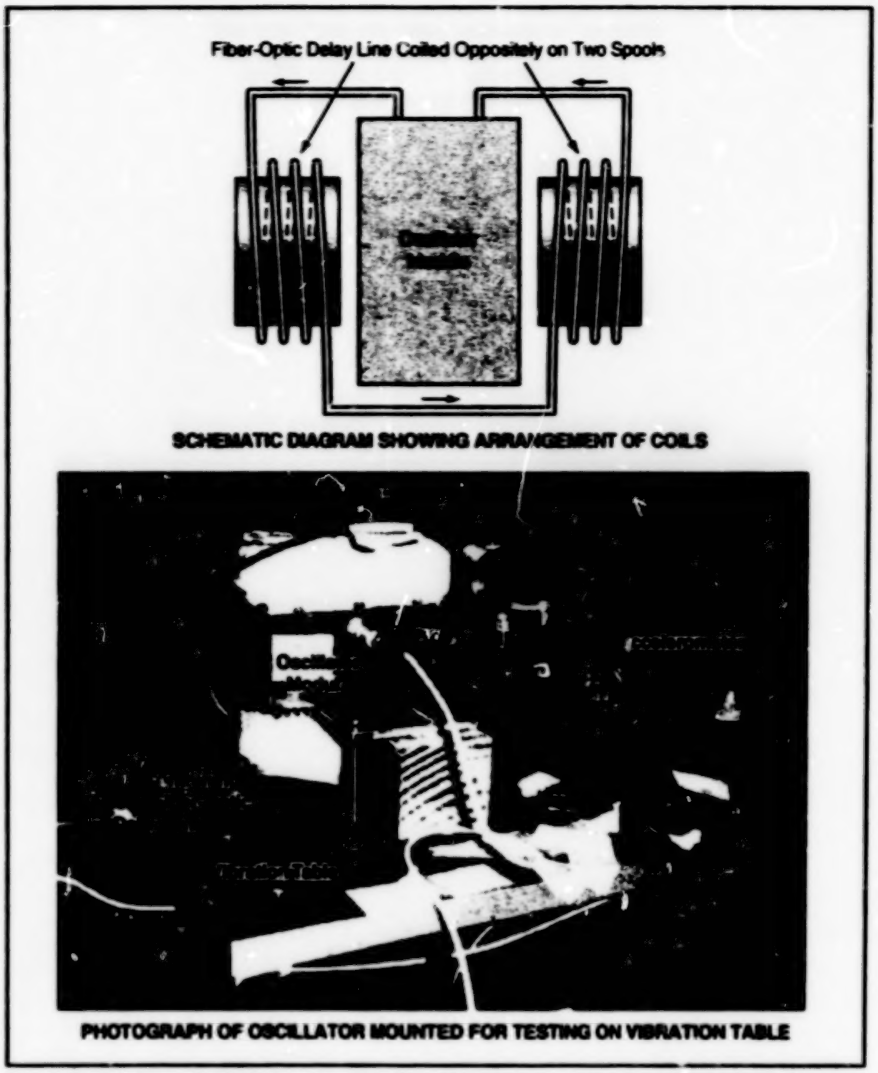

Figure 2. The Fiber-Optic Delay Line Has Been Split into two coils of opposite chirality. In combination with other features of design and construction, this split greatly reduces the sensitivity of the oscillator to acceleration along the coil axis.

Capacitors Containing Nanocrystalline $BaTiO_3$ as Dielectric

Energy densities, breakdown potentials, and resistances exceed those of prior $BaTiO_3$-dielectric capacitors.

John H. Glenn Research Center, Cleveland, Ohio

Capacitors in which the main dielectric layers are made from sintered nanocrystalline $BaTiO_3$ have been fabricated and tested in an initially successful and continuing effort to increase energy densities, breakdown potentials, and insulation resistances beyond those of prior commercial capacitors that contain coarser-grained sintered $BaTiO_3$. This development effort is based on the premise that the relevant physical properties of $BaTiO_3$ grains vary with their sizes in such a way that smaller grains are better suited for use as dielectrics in capacitors.

The variations in question can be summarized as follows:

- Capacitance and Energy-Storage Density: For reasons too complex to be explained in the limited space available for this article, hysteretic switching of ferroelectric domains in $BaTiO_3$ gives rise to a loss of capacitance and thus a loss of incremental energy-storage density with increasing applied potential. It had been conjectured that this detrimental effect of ferroelectric-domain switching could be minimized by reducing grain sizes to the nanocrystalline range (<100 nm). Thus, it should be possible to store more energy, especially near the upper limit of applied voltage for a given capacitor.
- Breakdown Potential and Energy-Storage Density: The breakdown

Property		Capacitors Made From Nanocrystalline $BaTiO_3$	Commercial Capacitors Made From Coarser-Grained $BaTiO_3$
Grain Size		<100 nm	0.5 μm
Relative Permittivity		1,815	2,498
Insulation Resistance at Applied Potential of 200 V	at Temperature of 25 °C	1,240 GΩ	132 GΩ
	at Temperature of 200 °C	730 MΩ	138 MΩ
Dielectric Breakdown	Potential/Thickness	863 V/8.75 μm	744 V/17.3 μm
	Electric Field Equiv. to Potential/Thickness	98.6 V/μm	43.0 V/μm
Energy-Storage Density at Half of Average Breakdown Potential		3.20 J/cm^3	1.86 J/cm^3

The Nanocrystalline-$BaTiO_3$ Capacitors were tested along with commercial $BaTiO_3$-dielectric capacitors and found to be superior with respect to insulation resistance, dielectric-breakdown electric field, and energy-storage density.

potential of $BaTiO_3$ or another ceramic dielectric material is related to its mechanical strength, which is approximately inversely proportional to the square root of the size of its smallest internal flaw. Inasmuch as the flaw size cannot be smaller than the grain size, it is expected that, along with mechanical strength, the breakdown potential should increase with decreasing grain size. The expected increase in the breakdown potential would contribute, along with the expected increase in capacitance, to an increase in achievable energy-storage density.

- Insulation Resistance: The insulation resistance of a capacitor is quantified by measuring the direct current that it passes when charged to a steady potential. A simplified electric model of a grainy dielectric material is that of grain-boundary and grain-interior elements in series. In a nanocrystalline (grain sizes less than about 100 nm) dielectric, more inherently resistive grain boundaries are present per unit thickness than are present in a coarser-grained version of the same material, and thus one expects the insulation resistance to be greater.

In preparation for testing these concepts, multilayer capacitors that contained sintered nanocrystalline dielectric layers were fabricated. The nanocrystalline dielectric materials were formulated to satisfy an Electronics Industries of America (EIA) standard, called X7R, that specifies acceptable ranges of dielectric properties as functions of temperature. Each grain of the X7R-compliant $BaTiO_3$ has a duplex microstructure comprising a lightly doped ferroelectric core surrounded by a heavily doped paraelectric shell. (The dopants are Bi, Nb, Zn, and Mn).

The table presents results of tests of capacitors made from one of the nanocrystalline-$BaTiO_3$ formulations and of commercially available capacitors made from coarser-grained $BaTiO_3$. These results clearly indicate the superiority of the nanocrystalline $BaTiO_3$ as the dielectric material. On the basis of these results and of other observations made during the tests, it appears that in comparison with capacitors made from coarser-grained $BaTiO_3$, capacitors made from nanocrystalline $BaTiO_3$ can operate more reliably at high temperatures and high voltages, can be made smaller and lighter for a given capacitance value, and can have higher energy-storage densities and higher capacitances for a given case size.

This work was done by John Freim and Yuval Avniel of Nanomaterials Research Corp. for **Glenn Research Center.**

Inquiries concerning rights for the commercial use of this invention should be addressed to NASA Glenn Research Center, Commercial Technology Office, Attn: Steve Fedor, Mail Stop 4–8, 21000 Brookpark Road, Cleveland, Ohio 44135. Refer to LEW-16984.

Electronic Systems

Hardware, Techniques, and Processes

BLANK PAGE

Vision-Only Operator Interface for a Robotic Manipulator

Images of the actual and commanded robot poses are displayed along with warnings.

NASA's Jet Propulsion Laboratory, Pasadena, California

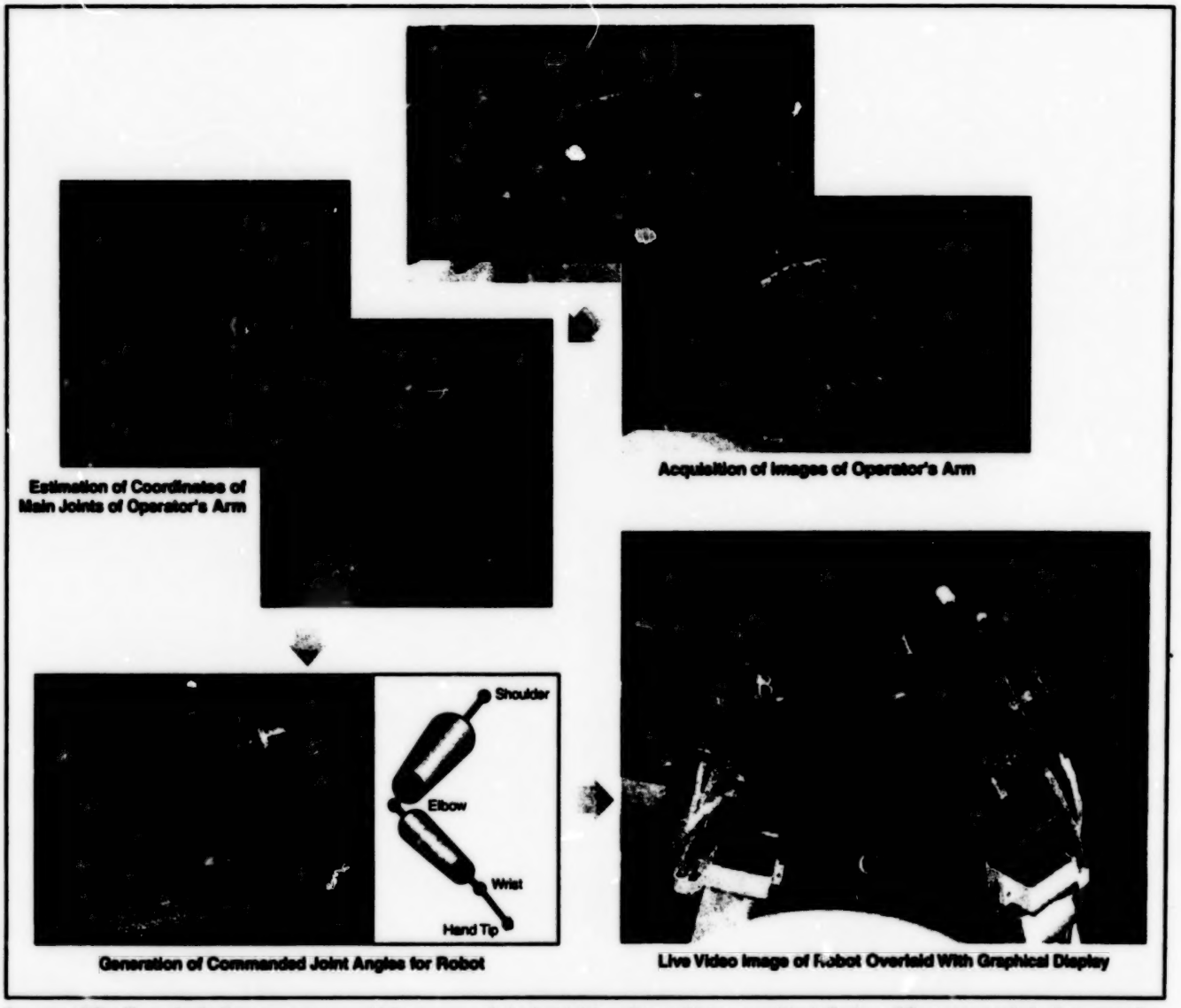

Images of the Operator's Arm are processed into commanded robot-joint angles and into a graphical display of the commanded robot pose plus warning icons overlaid on a video image of the robot.

A system of electronic hardware and software has been developed as an experimental prototype of a visual interface between a human operator and a possibly remote one-arm anthropomorphic robotic manipulator. The system is denoted, more specifically, as a vision-only operator interface to emphasize that unlike some other operator interfaces, it does not include joysticks, force-feedback devices, or other mechanical devices that could encumber the operator. The operator commands the robot by moving one of his or her arms; the operator receives feedback in the form of a live video image of the work space of the robot overlaid with a graphical model of the robot plus icons that warn of robot poses that should be avoided.

The figure is a simplified schematic depiction of the flow of data within the system and the sequence of actions performed by the system. The flow of data begins with acquisition of images of the operator's arms, by use of four video cameras that surround the operator. To facilitate tracking, the operator's space is darkened and the main joints (shoulder, elbow, and wrist) of the operator's arm are marked with small light bulbs. The image data from the video cameras are processed into three-dimensional Cartesian coordinates of the main joints at a video frame rate of 60 Hz, with an accuracy of 10 mm.

The coordinates of the main joints of the operator's arm are converted to commanded angles for joints of the robot arm. These commanded angles are used to construct the graphical model of the robot to be overlaid on the live video image of the robot. The model data are analyzed to detect self-collisions, which are defined here as situations in which two links of the manipulator come too close to each other. The links in danger of colliding with each other can be highlighted in the graphical display to help the operator avoid self-collisions; alternatively, lines indicating distances of closest approach can be drawn in the display.

In this system, the commanded joint angles are generated by use of the configuration-control formalism, which has been

described in a number of prior *NASA Tech Briefs* articles. The configuration-control formalism can resolve mathematical singularities associated with kinematic redundancies, but adds algorithmic singularities to robot poses that the operator would not easily recognize as being singular. Therefore, in the graphical display, the work space in the vicinity of the wrist of the robot arm is discretized into cubes, and each such cube is marked in red to indicate that a quantitative measure of the risk of a kinematic or algorithmic singularity at the center of that cube exceeds a specified threshold. The quantitative measure is the determinant of $J_A J_A^T$, where J_A is the augmented Jacobian determinant of the system, computed for the current orientation and the current manipulator arm angle (defined as the angle between shoulder/elbow/wrist plane and the vertical plane that contains both the wrist and the base of the robot).

This work was done by Paolo Fiorini, Eugene Chalfant, Pietro Perona, Enrico DiBernardo, and Yuichi Tsumaki of Caltech for NASA's Jet Propulsion Laboratory. Further information is contained in a TSP [see page 1].
NPO-20912

Ground-Traffic Information-Management System for an Airport

Real-time operational data are shared among diverse users to help minimize delays.

Ames Research Center, Moffett Field, California

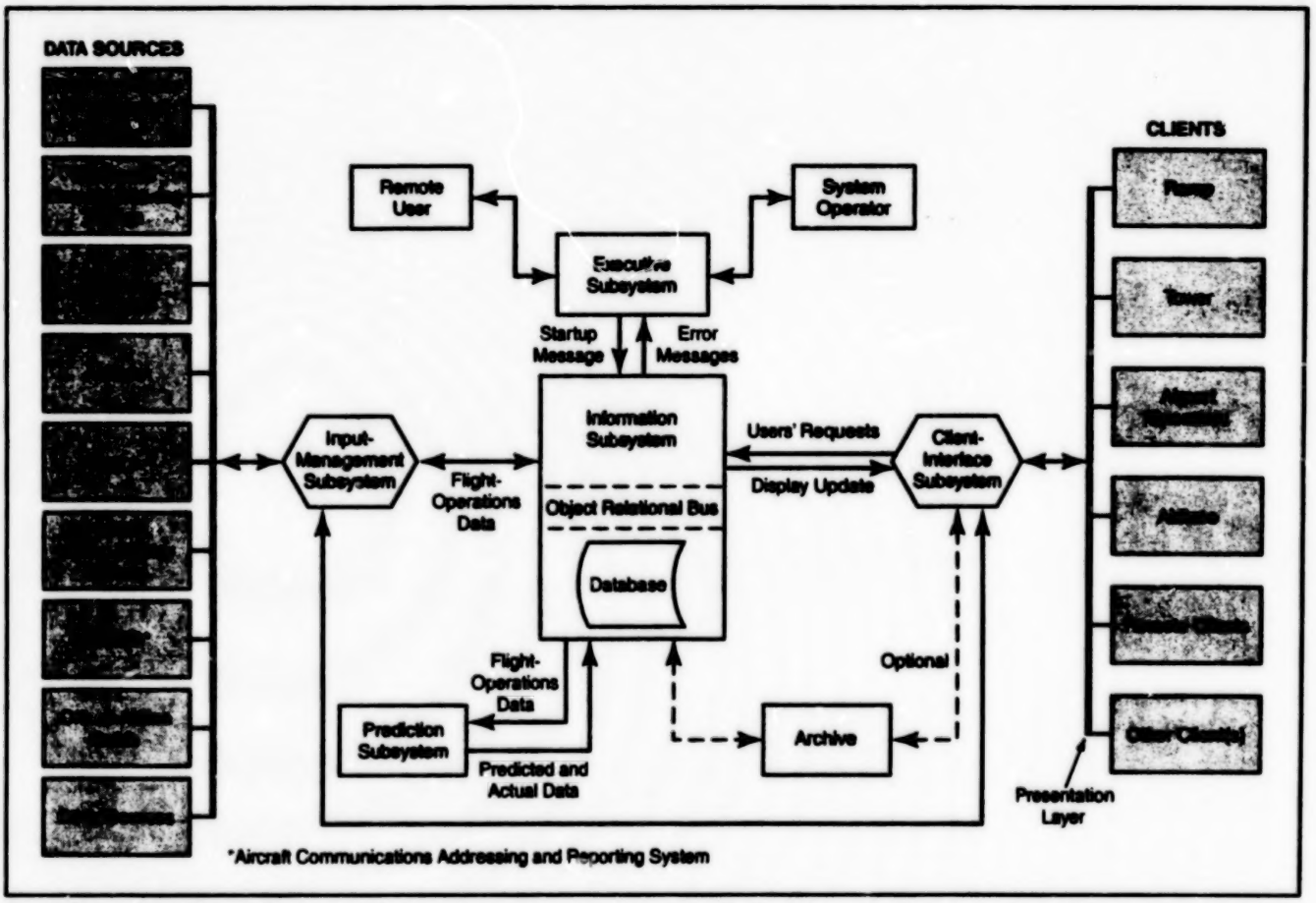

The TMS Is a Client/Server System that helps various user groups to increase the level of coordination of airport operations and thereby reduce ground-traffic delays.

A computer-based system, and a method built around the use of the system, have been developed to automate the acquisition, integration, and management of data that have been generated at different rates by multiple, heterogeneous, incompatible sources. The system [hereafter denoted the "TMS" (for "traffic-management system")] in its original form is intended for use in improving the management of ground traffic at a large, busy airport in order to reduce delays. The TMS could also be adapted to scheduling the movements of multiple vehicles in other settings — for example, vessels in harbors, trucks or railroad cars in shipping yards, and railroad cars in switching yards. Still other uses for the TMS could include managing containers at a shipping dock, managing stock on a factory floor or in a warehouse, and training of a variety of airline, airport, and government personnel in the management of airport ground traffic.

The basic TMS concept admits of variations. In a preferred representative version, the TMS is a client/server computer system that shares real-time aircraft-operations data among the Federal Aviation Administration (FAA), airlines, airport managers, and ramp controllers. The TMS (see figure) includes executive, information, input-management, prediction, and client-interface subsystems that are interconnected to participate in the interchange of real-time aircraft-operations data among the aforementioned groups. In addition to raising the level of coordination among these groups, the TMS generates its value-added data products for their use. These data products include estimated

times of arrival of airplanes at gates and estimated airplane-departure times. The TMS uses expert-system software to fuse data in order to establish and update reference data values for every aircraft surface operation.

The executive subsystem is responsible for controlling the other subsystems, starting and shutting down processes at scheduled times, monitoring system components for error and warning conditions, notifying system-support personnel of detected system errors, and, when possible, recovering from system failures. Additional duties of the executive subsystem include facilitating diagnoses of faults in subsystems, providing remote access for monitoring and control, maintaining system statistics, and managing user accounts. The executive subsystem can issue commands to reset various hardware components of the TMS.

The input-management subsystem is a collection of computer programs that handle the data coming in from various sources via network or serial links. In turn, the input-management subsystem feeds the data to the information subsystem.

The prediction subsystem is responsible for integrating all the input data in order to monitor the progress of arriving and departing flights, and to predict key events, including pushbacks (departures from gates), takeoffs, touchdowns, and arrivals at gates. The integrated monitoring information and predicted values are fed back to the information subsystem for display by the client-interface subsystem.

The client-interface subsystem is a collection of computer programs. In a preferred version of the TMS, the client-interface system distributes flight, TMS-status, and schedule data from the information subsystem to various clients, including the aforementioned sources of data and user groups and possibly other clients at remote locations. It also provides a graphical user interface for continuously displaying flight data on a bit-mapped display, and for executing various commands to change the data or the method of display.

This work was done by Brian J. Glass, Liljana Spirkovska, William J. McDermott, Ronald J. Reisman, James Gibson, and David L. Iverson of **Ames Research Center**. *Further information is contained in a TSP [see page 1].*

This invention has been patented by NASA (U.S. Patent No. 6,161,097). Inquiries concerning nonexclusive or exclusive license for its commercial development should be addressed to the Patent Counsel, Ames Research Center, (650) 604-5104. Refer to ARC-14268.

Millimeter-Wave and Microwave Treatment of Atherosclerosis

Controlled temperature profiles are generated to treat diseased coronary arteries without injuring them.

Lyndon B. Johnson Space Center, Houston, Texas

Millimeter-wave/microwave ablation (essentially, heating by use of millimeter-wave and microwave electromagnetic radiation) has been proposed as a means of treating atherosclerotic lesions. Computational simulations have shown that by controlling and customizing temperature profiles in millimeter-wave/microwave ablation, it should be possible to (1) treat atherosclerosis or coronary thrombosis without (2) incurring the distensions and injuries to arterial walls and epithelial walls that are common to current invasive treatments, while (3) possibly reducing post-treatment inflammation and even restenosis. Although millimeter-wave/microwave ablation has yet to be proved in tests on live animals, it offers the potential to significantly advance the state of the art. Indeed, after further testing, millimeter-wave/microwave ablation might be used by cardiologists during balloon angioplasty replacement procedures (PTCAs) or coronary catheterizations. Because it is expected to be safer and more effective than traditional methods, millimeter-wave/microwave ablation could soon supplement or even supplant today's treatment choices.

In millimeter-wave/microwave ablation, electromagnetic energy would be delivered via a catheter to a precise location in a coronary artery for selective heating of a targeted atherosclerotic lesion. Heating to controlled, customized temperature profiles could be used to treat lesions in the intima and media layers of an artery wall, yet the most superficial endothelial cell layer and the outer adventitial layer would be preserved. Preservation of the endothelial cell layer is necessary to prevent thrombotic, inflammatory, and proliferative processes (restenosis), which complicate angioplastic procedures.

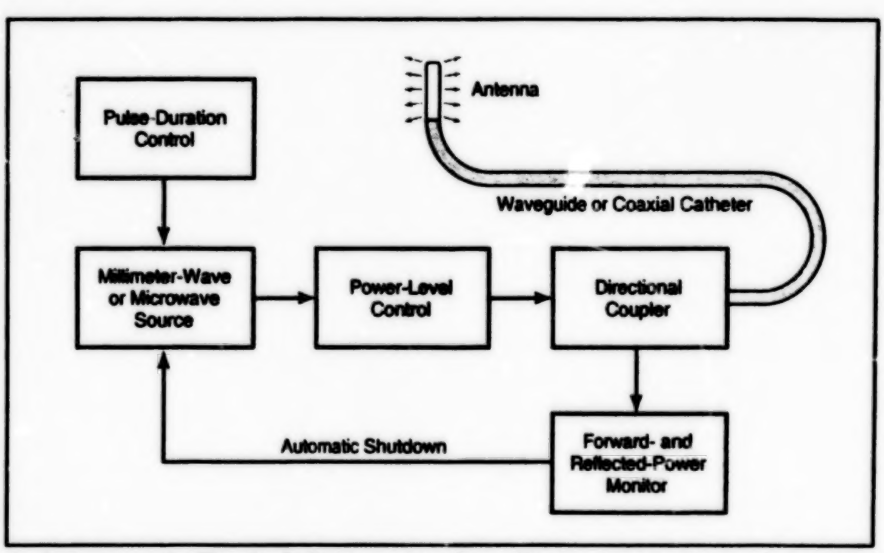

An Antenna on the Tip of a Catheter would radiate millimeter-wave or microwave energy to heat atherosclerotic lesions.

In millimeter-wave/microwave ablation, advantageous temperature profiles would be obtained by controlling the power delivered, pulse duration, and frequency. For best results, the profile would be chosen so that the maximum temperature is delivered at the center of an atherosclerotic lesion and the temperature would decrease, uniformly in all directions, with distance from the center. The heating would favorably modify lipid-rich lesions that contain the inflammatory cellular infiltrates that are prone to rupture, and the rupture of which causes thrombotic artery occlusions (heart attacks).

The major components of an apparatus for millimeter-wave/microwave ablation apparatus (see figure) would include a millimeter-wave/microwave source, a catheter/transmission line, and an antenna at the distal end of the catheter. The source would

generate millimeter-wave or microwave power at a controlled level up to 10 W, with a pulse duration between 0.1 and 10 s controlled to within 2 percent. A chosen frequency between 2 and 300 GHz could be used; a separate source would probably be needed for each frequency. The catheter/transmission line would deliver the power to the antenna.

The antenna would focus the radiated beam so that most of the millimeter-wave or microwave energy would be deposited within the targeted atherosclerotic lesion. Because of the rapid decay of the electromagnetic wave, little energy would pass into, or beyond, the adventitia. By suitable choice of the power delivered, pulse duration, frequency, and antenna design (which affects the width of the radiated beam), the temperature profile could be customized to the size, shape, and type of lesion being treated. By controlling temperature, one could limit (1) the damage to the endothelial layers and (2) the risk of overheating nondiseased tissue and proximal blood. For safety, the control system of the apparatus would provide automatic shutoff in the event of an inappropriate power level, excessive reflected power, unsuitable pulse duration, or heating beyond prescribed limits.

This work was done by Patrick Fink and G. D. Arndt of **Johnson Space Center**; *J. R. Carl and Reginald Beer of Lockheed Martin; George Raffoul of Hernandez Engineering, Inc.; and Philip Henry and Antonio Pacifico. Further information is contained in a TSP [see page 1].*

This invention has been patented by NASA (U.S. Patent No. 6,047,216). Inquiries concerning nonexclusive or exclusive license for its commercial development should be addressed to the Patent Counsel, Johnson Space Center, (281) 483-0837. Refer to MSC-22724.

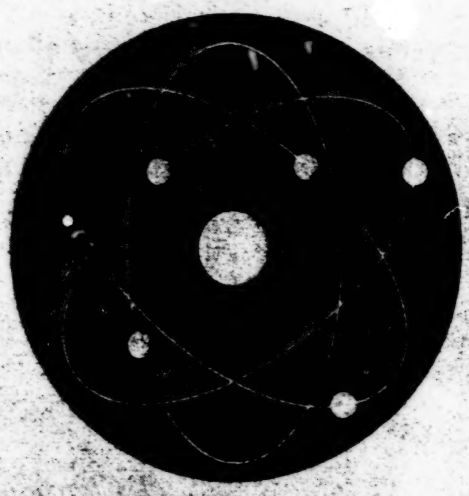

Physical Sciences

Hardware, Techniques, and Processes

Books and Reports

BLANK PAGE

Apparatus Measures X-Ray Diffraction and Fluorescence

A single apparatus performs functions for which two apparatuses were previously needed.

Ames Research Center, Moffett Field, California

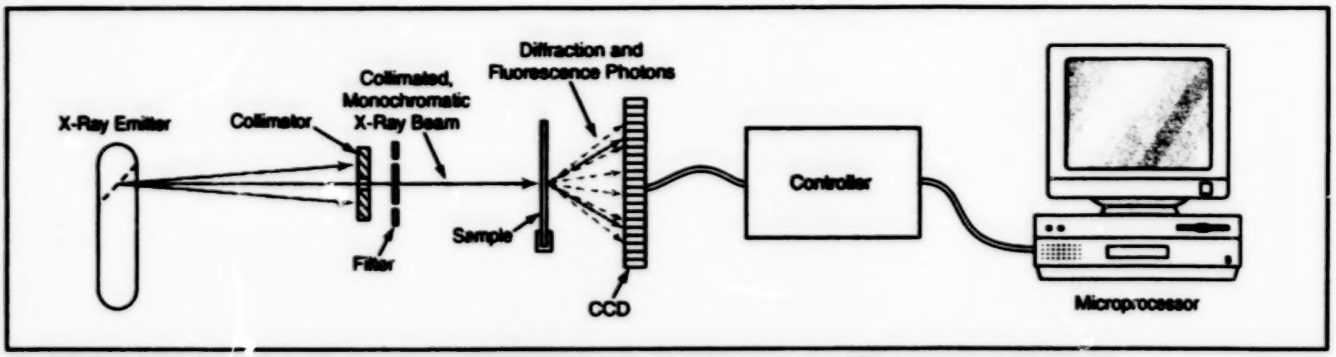

The Readout From the CCD in this apparatus yields information on the XRD pattern and XRF spectrum of the sample.

The figure depicts an apparatus for measuring x-ray diffraction (XRD) and/or x-ray fluorescence (XRF) in a specimen of material. The specimen could be, for example, a standard XRD powder sample of a mineral, the elemental composition of which one seeks to identify. It is common practice to characterize samples in terms of both XRD and XRF, but heretofore, it has been necessary to use separate XRD and XRF apparatuses.

The apparatus (see figure) includes a standard x-ray emitter — preferably one that generates x-rays at a number of photon energies. The x-ray beam from the source passes through a collimator, and the collimated beam passes through a band-pass filter, so that the sample is irradiated by a collimated, monochromatic beam.

The irradiated specimen emits mainly two kinds of x-rays: (1) primary (diffraction) photons at the incident photon energy; and (2) secondary (fluorescence) photons, which have lower energies. The photons emitted by the specimen travel to a charge-coupled device (CCD) containing a two-dimensional array of pixels, wherein the photons are detected. In general, the CCD pixel outputs depend on both the fluorescence spectrum and on the diffraction pattern projected onto the array of pixels. By suitable choice of the mode of operation, one can extract diffraction or fluorescence information from the CCD pixel outputs, as explained below.

Typical CCDs rival traditional Si(Li) detectors with regard to energy resolution and sensitivity in the energy range of 0.2 to 10 keV. Taking advantage of this characteristic, the CCD can be operated in a photon-counting mode; the CCD can be interrogated at such short intervals that in each successive interrogation, the output comprises indications of the energies of individual photons incident on single pixels. Taking further advantage of this characteristic, the CCD pixel outputs can be processed to select only those signals in a desired photon-energy range. The CCD pixel outputs are processed partly in a controller and partly in a microprocessor connected to a display unit.

The apparatus can be operated in any of several distinct modes, of which four are described below:

1. The sample is irradiated with a monochromatic beam and only the diffraction pattern is of interest. To discriminate against fluorescence photons, the CCD and the processing circuitry are operated so that only photons at the primary beam energy are counted in computing the diffraction pattern.
2. The sample is irradiated with a monochromatic beam and both diffraction and fluorescence are of interest. The CCD and processing circuitry are operated to measure both the primary and lower-energy photons. The diffraction pattern is extracted from the signals at the primary photon energy, while the fluorescence spectrum is extracted from the signals at lower photon energies.
3. The irradiating beam is monochromatic and only the fluorescence spectrum is of interest. In this mode, CCD outputs at the primary beam energy are rejected, and only the lower-energy signals are used in calculating the fluorescence spectrum.
4. The x-ray beam is polychromatic (a band-pass filter is not used), and only a particular diffraction pattern is of interest. In this mode, the CCD and processing circuits are operated to detect only diffraction at selected multiple beam energies and thus to discriminate against photons at all other energies. This mode is useful for diffraction experiments in which there is a need for fine adjustment of the x-ray beam energies to avoid strong absorption in the samples.

This work was done by David F. Blake, Charles Bryson, and Friedemann Freund of **Ames Research Center**. *Further information is contained in a TSP [see page 1].*

This invention has been patented by NASA (U.S. Patent No. 5,191,738). Inquiries concerning nonexclusive or exclusive license for its commercial development should be addressed to the Patent Counsel, Ames Research Center, (650) 604-5104. Refer to ARC-12043.

New Technique Improves Cirrus Cloud Characterization

Radiometric measurements at submillimeter-wavelength accurately characterize cirrus cloud properties.

NASA's Jet Propulsion Laboratory, Pasadena, California

A new technique for retrieving cirrus properties from radiometric measurements at submillimeter wavelengths has been developed. The technique can accurately measure the amount of ice present in cirrus clouds, determine the median crystal size, and constrain crystal shape. The retrieval algorithm improves upon prior algorithms by also retrieving middle and upper tropospheric water-vapor profiles in concert with cloud properties. This joint-analysis method corrects for retrieval errors introduced by

Experiment	IWP Decibel Error		D_{ms} Decibel Error	
	Median	Root Mean Square	Median	Root Mean Square
CEPEX, Zenith Looking, 10 Channels	1.2	2.3	0.7	1.1
CEPEX, Slant Upward Looking, 10 Channels	1.1	2.2	0.6	1.0
CEPEX, Zenith Looking, 11 Channels	0.8	1.8	0.6	1.0
FIRE II, Nadir Looking, 10 Channels	1.2	2.1	1.0	1.8

Errors Associated With Retrieval of IWP and D_{ms} are significantly reduced with the new retrieval technique.

water vapor in and near the cloud.

Submillimeter-wave cloud ice radiometry is a relatively new technique. In 1995, two theoretical papers were published describing the use of radiometry to characterize ice clouds. These studies indicated that cirrus clouds scatter the upwelling flux of submillimeter-wavelength radiation emitted by lower atmospheric water vapor back towards the Earth, thus reducing the upward flux of energy. (In the submillimeter-wave spectral region, ice particles primarily scatter radiation rather than emitting or absorbing it.) From space, this effect makes clouds look radiatively cold against the warm emissions of water vapor in the lower troposphere. The ability of cirrus ice to scatter radiation is primarily a function of the amount of ice and the distribution of crystal sizes. Scattering induced by changes in crystal size is distinguished from scattering induced by changes in the total ice content, termed the ice water path (IWP), by making measurements at widely spaced frequencies. Additionally, crystal shape can be constrained by determining the crystal height-to-width aspect ratio, which is derived from off-nadir measurements at orthogonal polarization angles. Key assumptions underlying the theoretical predictions were validated by a set of airborne measurements in 1996.

The new retrieval algorithm corrects for middle and upper tropospheric water vapor that degrades retrieval accuracy via two mechanisms. First, water vapor emits radiation, reducing the apparent fraction of the radiation scattered by an underlying cloud. Second, water vapor absorbs radiation, also reducing the apparent scattered fraction. Thus, there is a need for a retrieval technique that corrects for these water-vapor-induced screening effects. The new algorithm builds on previous work by simultaneously retrieving water-vapor profiles and cirrus properties.

A Bayesian algorithm is used to invert a mathematical model of the radiometric properties of both cloud ice and water vapor. The model is statistical in nature relying on a combination of an *in-situ* cirrus measurement database, assumptions about vertical cloud inhomogeneity, and estimates of cloud temperature. The *in-situ* cirrus database consists of measurements from four sets of field measurements including three sets taken over a tropical site (CEPEX) and one over a midlatitude, Midcontinent site (FIRE II). The assumptions about cloud inhomogeneity are based on the observed relationship between IWP and the median crystal diameter, D_{ms}.

The accuracy of this method has been assessed in computational simulations using the complement of radiometric channel planned for a new airborne instrument, the submillimeter-wavelength cloud ice radiometer (SWCIR) currently being developed by JPL. The instrument will have the capability to make radiometric measurements at ten frequencies spanning from 183 to 643 GHz. The simulations have quantified the accuracy of expected cirrus retrievals and have also quantified improvements that could be expected with the addition of an 880-GHz channel. The table presents selected results from these simulations. These results illustrate the dramatic improvement in accuracy that is achievable with the new analysis technique.

This work was performed by Steven Walter of Caltech (now employed by Aerojet in Azusa, CA), and K. Franklin Evans and Aaron Evans at the University of Colorado for **NASA's Jet Propulsion Laboratory.** *Further information is contained in a TSP [see page 1].*
NPO-21016

Books and Reports

Study of Inertial and Gravitational Masses of a Boson

A report presents a theoretical study of the relationship between the inertial mass (m_i) and gravitational mass (m_g) of a self-interacting neutral scalar boson in a heat bath. The question of whether these masses differ arises in modern physics. In quantum field theory, the mass of a particle appears as a parameter that, as a result of interaction with fields, is changed to a renormalizable, physically reliable value (m_R). The interaction of a particle with fields also has a thermal character. Thus, a boson in a heat bath in a gravitational field gains an acceleration different from the gravitational acceleration. The study utilizes a simple approximate Lagrangian model that is well suited for analysis of temperature- and gravitation-related effects. The full renormalized Feynman propagator of the boson is derived and used to find its Hamiltonian. The interaction with the gravitational field is introduced by using Tolman's equation to obtain the relationship between the local temperature and the local gravitational potential. From the resulting Hamiltonian, one obtains

$$m_g/m_i = 1 - (\lambda_R/12)(T_0/m_R)^2,$$

where λ_R is a renormalizable coupling constant and T_0 is the temperature at a position where the gravitational potential is zero.

This work was done by Igor Kulikov of Caltech for **NASA's Jet Propulsion Laboratory.** *To obtain a copy of the report, "Inertial and gravitational masses of bosons at finite temperatures," see TSP's [page 1].*
NPO-30325

Multiphase-Flow Model of Fluidized-Bed Pyrolysis of Biomass

A report presents additional information about the subject matter of "Model of Pyrolysis of Biomass in a Fluidized-Bed Reactor" (NPO-20708) *NASA Tech Briefs*, Vol. 25, No. 6 (June 2001), page 59. The model is built on equations for the dynamics of three components — gas, sand, and biomass — partly by taking suitable ensemble averages of the coupled conservation equations for the gas, and for the biomass and sand particles. Equations for exchanges of mass, momentum, and energy between phases are included. Equations for transport of the solid phase are closed by use of

separate distribution functions for sand and biomass particles. Interparticle collisions are described in the framework of the kinetic theory of dense gases, using inelastic-rigid-sphere models. The most important novelties of this model, relative to prior models, are (1) modeling of the stress tensor resulting from sand-biomass collisions, (2) the modeling of transfer of heat between phases and between particles in direct contact, and (3) modeling of multiple chemical reactions and the resulting transfer of mass between phases. The equations of the model are solved numerically.

This work was done by Josette Bellan and Danny Lathouwers of Caltech for **NASA's Jet Propulsion Laboratory**. *To obtain a copy of the report, "Multiphase Flow Equations for Modeling Tar Production from Biomass Particle Pyrolysis in a Fluidized Bed Reactor," see TSP's [page 1].*

NPO-20789

Metal/Dielectric Color Filters for Flat Panel Displays

A report expands on the proposal described in "Low-Absorption Color Filters for Flat Panel Display Devices" (NPO-20435) *NASA Tech Briefs*, Vol. 23, No. 12 (December 1999), page 34. To recapitulate: The dye pixel color filters in a conventional liquid-crystal or other display device would be replaced with interference filters, which are less absorptive, and optics would be configured so that light reflected from the filters would be reused as illumination. The overall effect would be to increase brightness and efficiency. The present report adds specificity by proposing that the interference filters be of the type described in "Metal/Dielectric-Film Interference Color Filters" (NPO-20217), *NASA Tech Briefs*, Vol. 23, No. 2 (February 1999), page 70: Each filter would be made of three thin metal films interspersed with two thin dielectric films. In comparison with conventional multilayer all-dielectric filters, the proposed filters would contain fewer layers, and therefore could be fabricated more easily and at lower cost.

This work was done by Yu Wang of Caltech for **NASA's Jet Propulsion Laboratory**. *To obtain a copy of the report, "Metal Film Interference Filter for Liquid Crystal Display Device," see TSP's [page 1].*

In accordance with Public Law 96-517, the contractor has elected to retain title to this invention. Inquiries concerning rights for its commercial use should be addressed to

Intellectual Property group
JPL
Mail Stop 202-233
4800 Oak Grove Drive
Pasadena, CA 91109
(818) 354-2240

Refer to NPO-20479, volume and number of this NASA Tech Briefs *issue, and the page number.*

BLANK PAGE

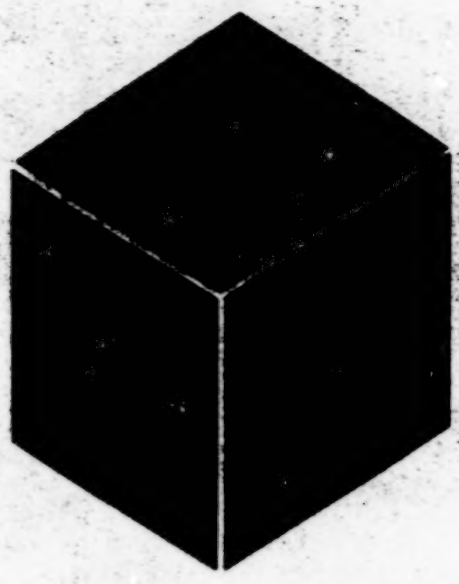

Materials

Hardware, Techniques, and Processes

BLANK PAGE

Fluorescent Dyes for Two-Photon Microscopy

Suitability for specific applications would depend on optical, chemical, and biological properties.

NASA's Jet Propulsion Laboratory, Pasadena, California

POTENTIAL CLASS-1 DYES:

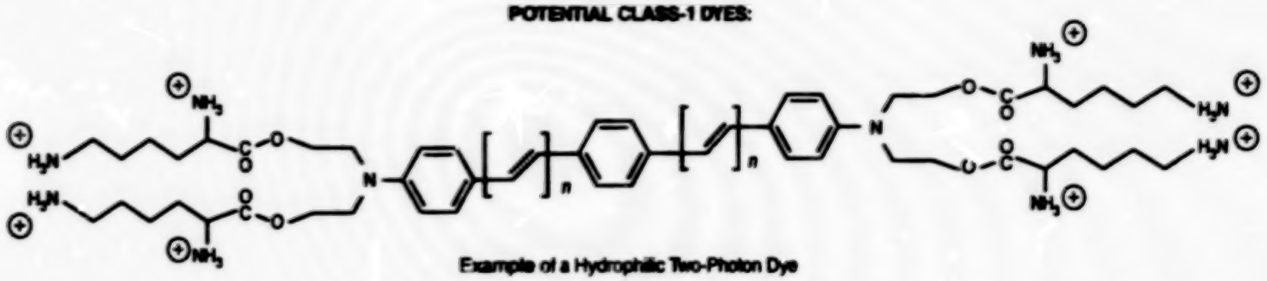

Example of a Hydrophilic Two-Photon Dye

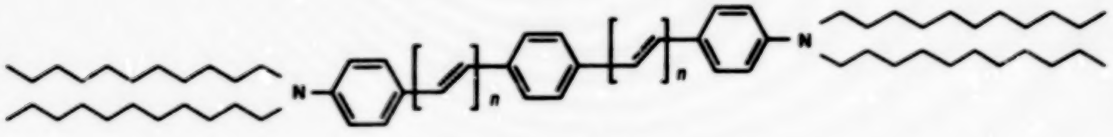

Example of a Lipophilic Two-Photon Dye

POTENTIAL CLASS-2 DYE:

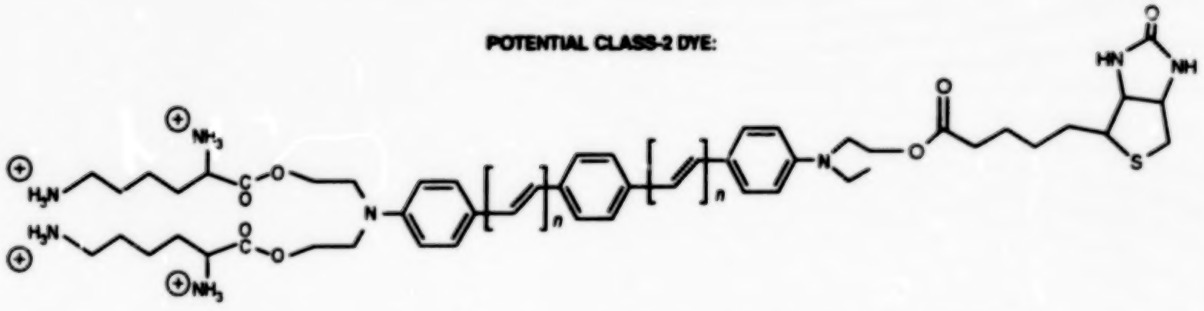

A Hydrophilic Two-Photon Dye for Antibody Attachment via Biotin/Avidin Complexation With Biotin-Tagged Antibody

These Dye Molecules have been identified as potentially suitable for use in two-photon microscopy.

A proposed program of research would be oriented toward the development of fluorescent dyes for use in two-photon microscopy. Two-photon microscopy and its predecessor, one-photon microscopy, are variants of fluorescence microscopy, which has become a major technology for biological and physical sciences. The basic idea in fluorescence microscopy is to use fluorescent compounds as markers for various physical and biological processes so that by observation of fluorescence under microscopes, one can locate those processes with high resolution in space and time. Because the fluorescence emitted by a compound can be isolated by its characteristic excitation and emission wavelengths, the compound can be traced with high signal-to-noise ratio, even in a "messy" environment. In two-photon microscopy, excitation of a fluorescent dye involves the concurrent absorption of two photons of approximately twice the wavelength of the peak of the single-photon-absorption spectrum.

During the past few years, two-photon microscopy has evolved to the incipient development of a commercial two-photon microscope. Heretofore, two-photon microscopy has been performed with dyes optimized for one-photon microscopy; these dyes are unlikely to satisfy the requirements for future relatively inexpensive two-photon microscopes, which are expected to feature simplified optics and power-efficient, ultrafast lasers combined in such a way as to afford only about 1/25 of the sensitivity of previously constructed prototype two-photon microscopes.

The dyes to be developed in the proposed research would be optimized for two-photon microscopy. Preliminary research has revealed that at least three classes of dyes will be needed:

1. Vital dyes could be used to label cells and follow them over time. These could include hydrophilic dyes that would be trapped in cytoplasm or hydrophobic dyes that would be carried in organelles or in cell membranes. Vital dyes must be optimized for minimal toxicity and slow bleaching.
2. Hydrophilic marker dyes would be formulated for covalent linking of antibodies for use in immunocytochemical labeling of tissues. These dyes could be based partly on vital dyes. However, because these marker dyes would be used on fixed tissue, toxicity would not be of concern as in the case of vital dyes. Marker dyes must be very hydrophilic to minimize the "background" staining that would otherwise occur because the dye would interact with, and stick to, the tissue. Marker dyes must be optimized for brightness; bleaching is of less concern.
3. Phototoxic agents would be used to sensitize cells or tissues for selective killing by laser light. A tumor or path-

ogen would be targeted, either by direct interaction with a dye or by formation of a targeting complex that could include, for example, antibodies to a tumor antigen. The dye-labeled tissue would be irradiated with light that the dye would absorb; photoactivated damage or toxic byproducts of dye bleaching would then kill the targeted cells. These dyes are required to be nontoxic until and unless illuminated.

The initial plan for the proposed research is straightforward, given that a few dyes (see figure) are already known to have properties that make them candidates for use in two-photon microscopy. These properties include absorption maxima in approximately the correct wavelength range and absorption cross sections about 50 times those of conventional dyes. The plan calls for the following coordinated efforts:

1. Synthesize dyes that (a) have two-photon-absorption wavelengths tuned for specific applications; (b) exhibit hydrophilicity suitable for control of biodistribution and, possibly, toxicity; and (c) are functionalized to provide for routine attachment to antibodies, caging complexes, and other biologically relevant compounds.
2. Determine lipo/hydrophilicity of each dye.
3. Measure two-photon cross sections at wavelengths from 780 to 1,000 nm, determine one- and two-photon-fluorescence quantum efficiencies, and characterize bleaching rates and byproducts.
4. Test each dye in a biological setting to determine toxicity with and without illumination and to determine performance under a microscope.

This work was done by Scott E. Fraser, Seth R. Marder, and Joseph W. Perry of Caltech for **NASA's Jet Propulsion Laboratory**. *Further information is contained in a TSP [see page 1].*

In accordance with Public Law 96-517, the contractor has elected to retain title to this invention. Inquiries concerning rights for its commercial use should be addressed to

Intellectual Property group
JPL
Mail Stop 202-233
4800 Oak Grove Drive
Pasadena, CA 91109
(818) 354-2240

Refer to NPO-20150, volume and number of this NASA Tech Briefs *issue, and the page number.*

Testing Soil for Electrokinetically Enhanced Bioremediation

Data from tests provide guidance for *in situ* treatment.

John F. Kennedy Space Center, Florida

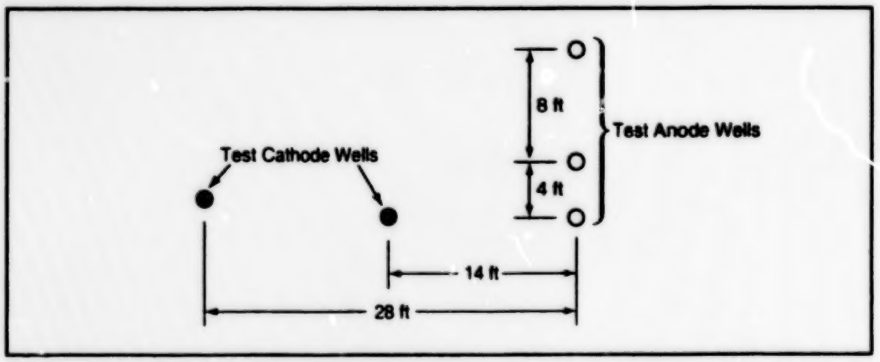

Test Cathode and Anode Wells can be positioned in this pattern or any of a variety of other patterns, depending on the size and nature of the soil region of interest. The minimum number of electrode wells needed for a prefield test is three.

The term "prefield test" denotes an *in situ* test of contaminated soil in preparation for *in situ* treatment of the soil by a method called "electrokinetically enhanced bioremediation" (EEB). A prefield test yields data that are helpful in designing and operating an efficient and cost-effective EEB system.

EEB was described in "Engineered Bioremediation of Contaminated Soil" (KSC-12045), *NASA Tech Briefs*, Vol. 25, No. 7 (July 2001), page 58. To recapitulate: EEB involves the utilization of controlled flows of liquids and gases into and out of the ground via wells, in conjunction with electrokinetic transport of matter through pores in the soil, to provide reagents and nutrients that enhance the natural degradation of contaminants by indigenous and/or introduced microorganisms. An EEB system includes injection and electrode wells, pumps, reservoirs of chemicals, and other components needed to control the movements of charged anionic and cationic as well as noncharged chemical species and microorganisms through the ground.

It has been standard practice, in preparing to design systems for *in situ* treatment of contaminated soil, to perform bench-scale laboratory tests on samples of soil from contaminated sites to determine hydrogeological, physical, and chemical parameters of soils and contaminants. A prefield test yields additional information that cannot be obtained from a bench-scale test and thus makes it possible to design a superior treatment system for a specific contaminated site. The additional information pertains to electrical conductivity and other parameters that vary spatially because of spatial variations in such properties of the soil as porosity, density of packing of particles, and chemical properties of pore fluid/soil interfaces. The data from a prefield test make it possible to optimize such design and operating parameters as applied voltages and currents and the positions of electrode wells, in order to treat the contaminated soil efficiently and more nearly uniformly.

In preparation for a prefield test, one inserts multiple test electrodes at different locations dispersed over the soil region of interest. At least one test electrode must be an anode and at least one must be a cathode (see figure). During the test, known dc voltages and currents are applied to the soil via the test electrodes. Voltage probes are inserted in the soil at various depths and at numerous horizontal positions between the test electrodes. The voltage readings as functions of position are used to generate a three-dimensional map of the test electric field.

The inhomogeneities of the test electric field are related to the inhomogeneities of the soil and the positions of the test electrodes, and can be used to guide the subsequent placement of working electrode wells for remediation of the soil. A rule of thumb calls for the placing the working electrode wells so that at locations far from the electrode wells but still within the region of soil to be treated, the electric field should be at least 10 to 20 percent as strong as the electric fields near the electrode wells.

Other parameters can also be measured during a prefield test:

- It can be useful to measure the temperature of the soil at various positions between the test electrodes and the temperatures of the test electrode wells as functions of applied currents.
- The volumes of fluids in the electrode wells can be measured over time to determine rates of electro-osmotic flow through the soil. It may also be useful to track rates of electro-osmotic flow functions of applied voltages.
- Voltage drops across electrode-well walls can be measured for use in determining the optimum well-wall materials for particular soil conditions.
- The pH of the soil near a test electrode well can be measured while releasing a pH-adjusting solution from the well at a known rate. The result of this measurement provides guidance for adjusting the pH of the soil during treatment.

This work was done by Dalibor Hodko of Lynntech, Inc., for **Kennedy Space Center**. *Further information is contained in a TSP [see page 1].*

In accordance with Public Law 96-517, the contractor has elected to retain title to this invention. Inquiries concerning rights for its commercial use should be addressed to

Dalibor Hodko
Lynntech, Inc.
7610 Eastmark Drive
Suite 202
College Station, TX 77840
(979) 693-0017

Refer to KSC-12160, volume and number of this NASA Tech Briefs *issue, and the page number.*

Crystalline Organic Films for Optical Applications

Nonlinear optics can be implemented as smaller, less power-hungry devices.

Marshall Space Flight Center, Alabama

Cells that contain thin, single-crystal films of photoresponsive organic materials [e.g., meta-nitroaniline (m-NA)] have been invented for use as nonlinear optics and especially as second-harmonic generators. In comparison with crystals of potassium dihydrogen phosphate (KDP) that have been used previously in such applications, the crystals of this invention are smaller and are capable of producing second harmonics of input light at lower input power levels.

A cell according to the invention (see figure) includes an upper and a lower plate made of fused quartz or other transparent material. A recess to hold the organic material is formed in the lower plate. The recess includes a groove around its periphery. The upper surface of the lower plate, the broad upward-facing surface of the recess, and the lower surface of the upper plate are optically polished to (1) eliminate defects that would otherwise act as seeds for undesired nucleation of multiple crystals in the final crystallization process described below and (2) enable the upper and lower plates to fit closely together. The dimensions of the final organic crystal are determined by the dimensions of the recess — typically a diameter of the order of 10 mm and a thickness between 0.5 and 500 μm.

The quantity of the organic material placed in the recess is chosen so that the material fills all of the recess except for the groove; this is because the groove serves to absorb any excess of the organic material during melting and/or thermal expansion, to prevent the material from flowing between (and thereby forcing apart) the faying surfaces of the upper and lower plates. Once the organic material is placed in the recess, the upper and lower plates are put together. The resulting cell containing the organic material is heated to melt the organic material, then cooled to freeze the organic material in a polycrystalline form with an even distribution of grains.

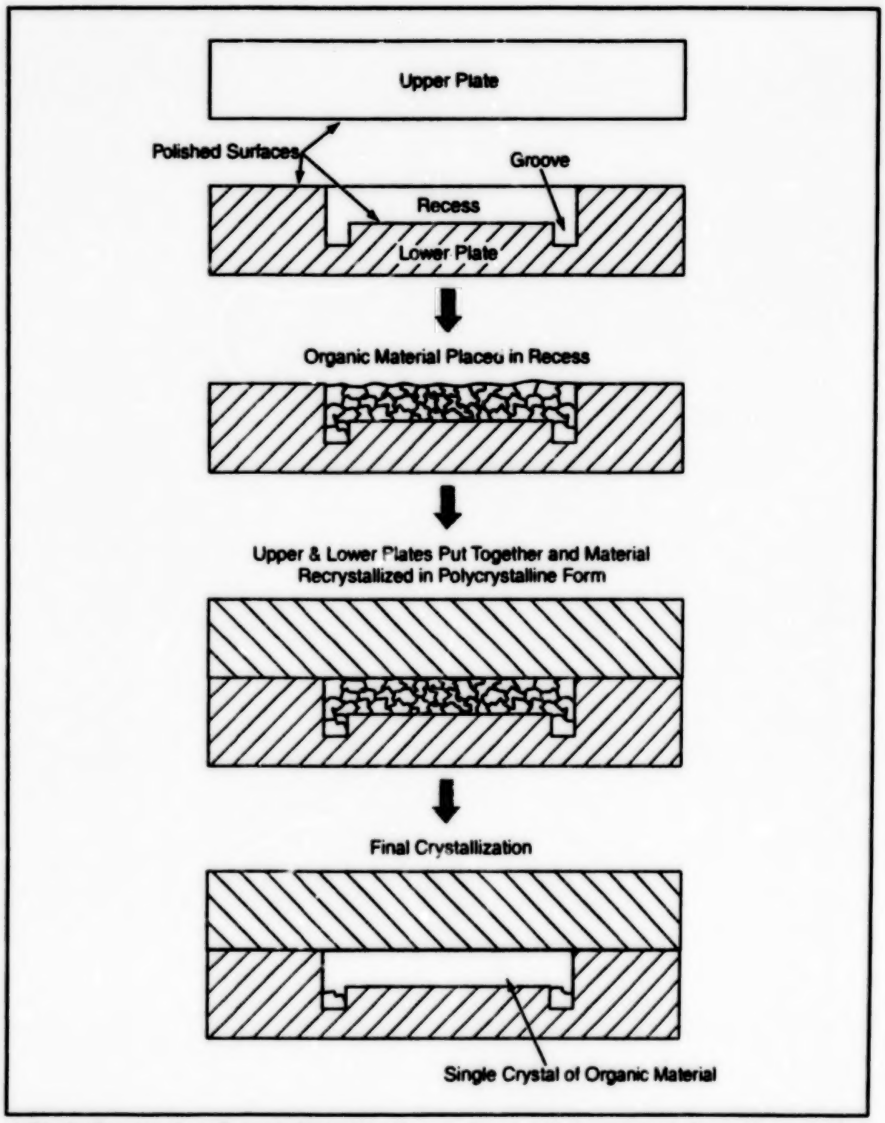

A Single Crystal of an Organic Material with a nonlinear optical response is formed by controlled solidification in a recess between two optically polished transparent plates.

The cell is then placed on a controlled-temperature, heated stage under a polarizing microscope, so that the organic materi-

al can be heated and cooled for the final crystallization and the microscope can be used to observe the crystallization process. The temperature of the stage is first increased to the melting point, taking care that except for a single seed crystal of desired orientation, all the organic material is melted. The seed crystal can be singled out under the microscope, and while all other crystals melt, it can be kept solid by exposing it to a microjet of cool air. The temperature of the stage is then slowly decreased, causing the organic material to freeze as a single crystal that grows outward from the seed crystal.

This work was done by Alexander Leyderman of the University of Puerto Rico for **Marshall Space Flight Center**. *For further information, please contact the innovator at alex@feynman.upr.clu.edu.*

Inquiries concerning rights for the commercial use of this invention should be addressed to the Patent Counsel, Marshall Space Flight Center [see page 1]. Refer to MFS-31450.

Critical Composition Buffering for Growing $In_xGa_{1-x}As$ on InP

Improved buffer structure for lattice-mismatched InGaAs devices.

John H. Glenn Research Center, Cleveland, Ohio

A method of growing lattice-mismatched $In_xGa_{1-x}As$ epitaxial layers on InP substrates using intermediate buffer layers of $InAs_yP_{1-y}$ has been invented to improve the performance of $In_xGa_{1-x}As$ thermophotovoltaic devices. The use of buffer layers is required to minimize the density of threading dislocations generated because of the lattice mismatch between low-bandgap $In_xGa_{1-x}As$ and InP. These defects degrade the electrical performance of the InGaAs device by acting as recombination centers for minority carriers.

The traditional approach to buffer layer design strives to accommodate the stress developed by the lattice mismatch through generation of misfit dislocations that are confined to the substrate/epilayer interface, while minimizing the generation of threading dislocations that propagate through the epitaxial layer(s). Often, many buffer layers, strained layer superlattices (SLS) or thermal cycle growth techniques are used to increase the interaction of threading dislocations, thereby reducing the overall dislocation density. The method described here utilizes different phenomena first observed in InGaAs grown on GaAs, whereby the strain of lattice mismatch is accommodated by dislocation formation in the substrate and underlying buffer layers rather than the top device epilayers. The success of this method depends on the selection of the composition of each buffer layer according to several criteria, most notably the following:

- The yield strength of each buffer layer must exceed that of the adjacent lower layer (including that of the substrate) so that dislocations are preferentially generated in the softer, lower layers.
- The buffer layers must be in compression, relative to the substrate.
- The compositions of the buffer layers must be chosen to make the lattice mismatch between any two adjacent layers less than a critical value, below which few or no dislocations propagate up through the layers to the overlying $In_xGa_{1-x}As$. This translates to making the compositions of the adjacent buffer layers differ by less than a corresponding critical amount.

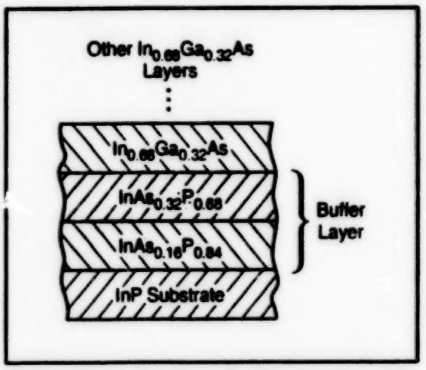

Only Two $InAs_yP_{1-y}$ Buffer Layers with carefully chosen values of *y* are needed to bridge the lattice mismatch between the InP substrate and the first $In_{0.68}Ga_{0.32}As$ layer.

It has been seen that the yield strength of an alloy of two materials varies with composition, with the maximum occurring at a 50/50 mixture. For example, it has been suggested that the yield strength of InGaAs has a maximum at a composition of $In_{0.5}Ga_{0.5}As$ (at elevated temperatures characteristic of epitaxial growth). The use of InGaAs buffer layers for the growth of low bandgap (i.e., 0.6 eV) $In_{0.68}Ga_{0.32}As$ on InP may begin with a $In_{0.53}Ga_{0.47}As$ buffer layer lattice-matched to the InP substrate and be comprised of InGaAs layers with increasing In content and lower yield strength. Thus, the buffer layer structure begins with a strong material followed by successively weaker materials. Stress tends to be relieved by dislocation formation in the weaker overlying layers. The opposite is true for buffer layers composed of $InAs_yP_{1-y}$. The buffer structure begins with InP and proceeds with successively higher yield strength material, thereby encouraging the formation of threading dislocations in the underlying materials. Cross-sectional TEM (transmission electron microscopy) analysis has verified this behavior of $InAs_yP_{1-y}$ buffer layers on InP. This technique allows buffer layers to be produced with fewer and thinner layers providing cost and operational benefits.

The figure depicts the buffer-layer structure of a typical $In_xGa_{1-x}As$ thermophotovoltaic device fabricated by the present method. In this case, *x* is chosen to be 0.68 to obtain a bandgap of 0.6 eV. Only two $InAs_yP_{1-y}$ buffer layers are needed: For the first buffer layer, *y* is chosen to be 0.16 to obtain a lattice mismatch of 0.58 percent with the substrate. For the second buffer layer, *y* is chosen to be 0.32 to obtain both a lattice mismatch of 0.51 percent with the first buffer layer and a lattice match with the first $In_xGa_{1-x}As$ layer.

This work was done by David Wilt of **Glenn Research Center** *and Richard W. Hoffman of Essential Research, Inc. Further information is contained in a TSP [see page 1].*

Inquiries concerning rights for the commercial use of this invention should be addressed to NASA Glenn Research Center, Commercial Technology Office, Attn: Steve Fedor, Mail Stop 4–8, 21000 Brookpark Road, Cleveland, Ohio 44135. Refer to LEW-16776.

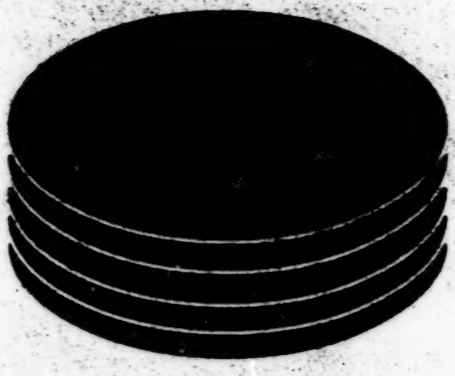

Computer Programs

Mechanics

Mathematics and Information Sciences

BLANK PAGE

Mechanics

Software for Analyzing Valve-Actuator Performance

A computer program assists engineers in analyzing data on the performances of actuators of fuel and oxidizer valves in the main engines of the space shuttle. The program could be adapted to similar use in other settings in which, as in the space shuttle, valve actuators are instrumented to provide data on commanded versus actual actuator positions. The program acquires such data during a specified diagnostic procedure in which valves are opened and closed. The program processes the data and generates several indications of performance, including trend plots, delta command minus actual positions plots, ramp-rate plots, error-from-command plots, and the means and standard deviations of the plotted quantities. The advantage afforded by the program is that it gives more information than does a simple pass/fail testing criterion. By looking at engineering performance profiles generated by this program during tests performed at different times, the engineers can identify valves that are about to fail in time to replace them.

This program was written by Edwin A. Cortes of **Kennedy Space Center**.
KSC-12238

Mathematics and Information Sciences

Software for Network Processing of Work Orders

The Electronic Portable Information Collection (EPIC) computer program is a computer system that processes work authorization documents (WADs). The EPIC System, which is also known as the Portable Data Collection System, comprises a central data server and portable data terminals. The central data server acts as the host on a local-area network and maintains the WAD data in Structured Query Language (SQL) and a database. The portable data terminals are desktop, laptop, and pen-based tablet computers that run, variously, the Windows 95 or Windows NT operating system and are connected to the central data server via the network.

In the current process that the EPIC system is designed to replace, all data pertaining to a job to be done by a team of workers are recorded on one master paper copy of the WAD for that job. Each member of the team has a paper copy, on which is recorded information pertinent to the task(s) to be performed by that member. Entries on the paper documents are authenticated by use of ink stamps. The person who holds the master copy of the WAD is the only one who has immediate access to a complete record of all processing that takes place, including deviations incorporated into the WAD.

In the EPIC system, task steps, deviations, and other pertinent data are stored in the SQL database, which is read and written by use of the EPIC software. Stamping is performed electronically; that is, the aforementioned data include information that serves the purpose now served by ink stamps. By use of the EPIC software, WADs can readily be stored, retrieved, and run on-line.

The EPIC software includes the following modules:

- *Form Conversion Module*
  Prior to execution of the job described in a WAD, this module is used to extract the data from the WAD (which is a Microsoft Word document) and insert the data into the database.
- *Stamp Utilities Module*
  This module administrates the electronic stamps. It associates the electronic stamps with the data in the database, including the user's name, and the user's telephone, fax, office, and identification numbers. It also associates the stamp with the authentication image of the work stamp assigned to the person who performed the task to which the stamp pertains.
- *Report Generator Module*
  After completion of a job, this module generates an as-run report. The report includes all of the information from the original version of the WAD plus the stamps, notes, deviations, and other data that were entered during the job. The report is put into Portable Document Format (PDF); as such, it is a read-only document that can be searched. Clean reports, which consist of the original WAD plus deviations but no stamp or data entries, can also be generated.
- *Portable Data Terminal Module*
  This module provides a graphical user interface (GUI) for displaying the information on, and entry of information into the system from, the portable data terminal of a member of the team. A member can enter task data by use of a keyboard, mouse, or electronic pen. A member can alter work procedures by use of a deviation form through which the WAD can be edited and approvals for changes can be obtained. As information is thus entered via a portable data terminal, it becomes immediately available on all the other portable data terminals.

This program was written by Kathy Potter, John Lekki, and Carl I. Delaune of **Kennedy Space Center** *and Mike Kappel of Sentel Corp. For further information, see below.*

In accordance with Public Law 96-517, the contractor has elected to retain title to this invention. Inquiries concerning rights for its commercial use should be addressed to

Raymond Babineau
Sentel Corp.
PO Box 1399
Dahlgren, VA 22448
(504) 663-0471
E-mail: rbabineau@sentel.com

Refer to KSC-12172, volume and number of this NASA Tech Briefs *issue, and the page number.*

Program Injects Random Faults for Testing Computers

JIFI (Jet Propulsion Laboratory's Implementation of a Fault Injector) is a computer program for studying the ability of a computer to tolerate, detect, and/or recover from faults (that is, bit errors). JIFI affords the capability to inject faults into user-specified central-processing-unit (CPU) registers and memory regions with uniform random distributions in location and time. This capability makes it possible to study the fault sensitivity of either a computer regarded as a complete system or of a specified component of hardware or application software. JIFI operates at the application level and is easy to use. In contrast, prior fault-injection software operates at a lower level and is more difficult to use. JIFI includes fault-injection, profiling, output-verifying, and

classifying subprograms that constitute parts of an easy-to-use software interface for performing fault-injection experiments and analyzing the resulting data. JIFI generates a fault-injection-result output file for each run. Data from massive fault-injection campaigns can be collected and processed automatically.

This program was written by Anil Agrawal, Garen Khanoyan, John Beahan, Leslie Callum, Raphael Some, and Won Kim of Caltech for **NASA's Jet Propulsion Laboratory**. *Further information is contained in a TSP [see page 1].*

This software is available for commercial licensing. Please contact Don Hart of the California Institute of Technology at (818) 393-3425. Refer to NPO-30162.

Software for Geometric Calibration of Video Cameras

A software library and set of programs largely automate the geometric calibration of video cameras. Developed especially for robotic vision systems, this software generates the information needed to determine the three-dimensional (3D) positions of objects that appear in two-dimensional (2D) video images. Typically, the software can perform 2D-to-3D mappings with precision of 0.1 to 0.3 pixels. The software enables the creation, manipulation, and application of geometric models of camera lenses. The models are constructed semiautomatically from images of known calibration targets, and these models can be applied automatically to live images, thereby enabling robots to generate the position information needed for such robotic operations as manipulation of objects, mapping, and navigation. The software supports three main types of models: (1) linear (ordinarily suitable for fields of view narrower than about 30°), (2) radial lens distortion (typically suitable for fields of view ranging from 15° to 110° wide), and (3) fisheye lens distortion (typically suitable for fields of view wider than 90°). Camera models generated by this software have enabled the development of real-time, vision-based control systems on a variety of advanced civilian and military robots.

The algorithms and software were developed by Don Gennery, Todd Litwin, Yalin Xiong, Mark Maimone, and Larry Matthies of Caltech for **NASA's Jet Propulsion Laboratory**. *Further information is contained in a TSP [see page 1].*

This software is available for commercial licensing. Please contact Don Hart of the California Institute of Technology at (818) 393-3425. Refer to NPO-21077.

KPP — a Preprocessor for VHDL

KPP is a computer program that serves as a preprocessor for VHDL code. [VHDL signifies VHSIC Hardware Description Language, which is a language used by the United States Department of Defense for describing, designing, and simulating very-high-speed integrated circuits (VHSICs).] KPP is based on, and similar to, CPP, which is a preprocessing program for the C computing language. KPP adds certain features that are useful to digital design engineers but are lacking in VHDL. These include, most notably, a capability for nested looping. KPP also provides a number of standard functions for defining and undefining variables, incorporating contents of named files, conditional execution of instructions, and block comments. The use of KPP can enable faster coding and greater reuse of designs. KPP can run in the Windows 95, Windows 98, and Windows NT operating systems.

This program was written by Richard Katz of **Goddard Space Flight Center** *and I. Brill of Edutech, Inc. Further information is contained in a TSP [see page 1].*
GSC-14380

Mechanics

Hardware, Techniques, and Processes

BLANK PAGE

Tip Fences for Reduction of Lift-Generated Airframe Noise

These simple, easily retrofitted devices reduce drag as well as noise.

Ames Research Center, Moffett Field, California

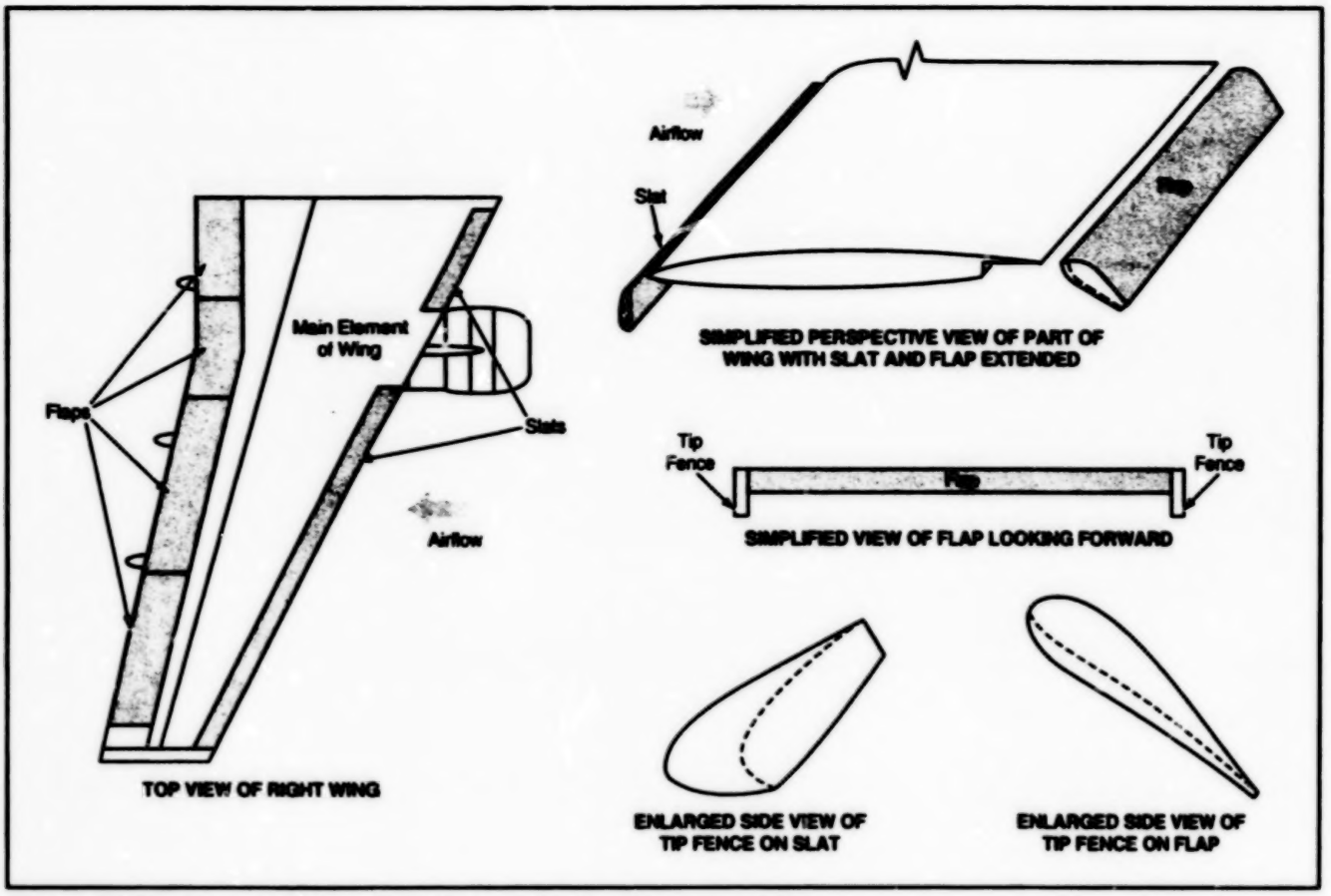

Figure 1. Tip Fences can readily be added to flaps and slats to reduce noise and drag.

Tip fences have been invented to reduce the noise generated in the airflows about the high-lift systems (the flaps and slats) of airplane wings. Tip fences also afford an important secondary benefit by increasing lift-to-drag ratios.

Typical modes of operation of the flaps and slats of an airplane wing are the following: In preparation for takeoff, the flaps are partly extended, and the slats are fully extended to provide a clean airflow over the main element of the wing. Shortly after takeoff, the slats are retracted to increase the lift-to-drag ratio during climbout. During landing, the slats and flaps are fully extended, and significant aerodynamic noise is generated at their tips. Tip fences can reduce the noise generated during takeoff and climbout, but more importantly during approach and landing.

Tip fences are so named because they are fencelike barriers and are mounted at or near some or all of the inboard and outboard tips of the flaps and slats (see Figure 1). These mounting locations are chosen because they are as close as possible to the aerodynamic-surface discontinuities where vortices associated with noise form when flaps and slats are extended. Tip fences can be made of any suitable rigid material (e.g., metal or composites) and can be attached to the tips of

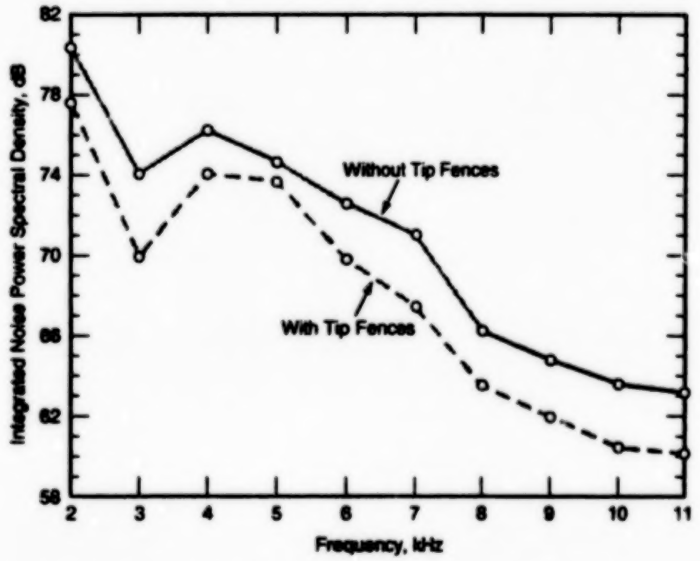

Figure 2. Less Noise Was Generated by the airflow over a wing equipped with flap tip fences than by the airflow over same wing without flap tip fences under otherwise identical test conditions.

flaps and slats by riveting, welding, bolting, or other conventional means. They can be easily and inexpensively retrofitted to most pre-existing airplanes, with minimal design changes.

A tip fence can be formed from a flat plate, or, if desired, it can be fabricated as a more complex, aerodynamically contoured body. In a typical application, the tip fences would extend below the lower surface of a slat or flap, as depicted on the right side of Figure 1. However, other combinations of tip and fence configurations are also possible.

In a demonstration of the benefits of tip fences, two different versions of a wing with flap extended were tested in a wind tunnel and in flight on a Lanceair IV airplane. In one version, the flap was equipped with tip fences; in the other version, it was not. The flight data is shown in Figure 2, demonstrating that the tip fences caused less noise to be generated over a broad range of frequencies. The wind-tunnel data showed that tip fences can also reduce the profile or viscous drag significantly.

This work was done by James C. Ross and Bruce L. Storms of **Ames Research Center**. *Further information is contained in a TSP [see page 1].*

This invention has been patented by NASA (U.S. Patent No. 5,738,298). Inquiries concerning nonexclusive or exclusive license for its commercial development should be addressed to the Patent Counsel, Ames Research Center, (650) 604-5104. Refer to ARC-14009.

Compact, Stiff, Lightweight, Quick-Release Clamp

This clamp offers several advantages over a prior toggle-action clamp.

Lyndon B. Johnson Space Center, Houston, Texas

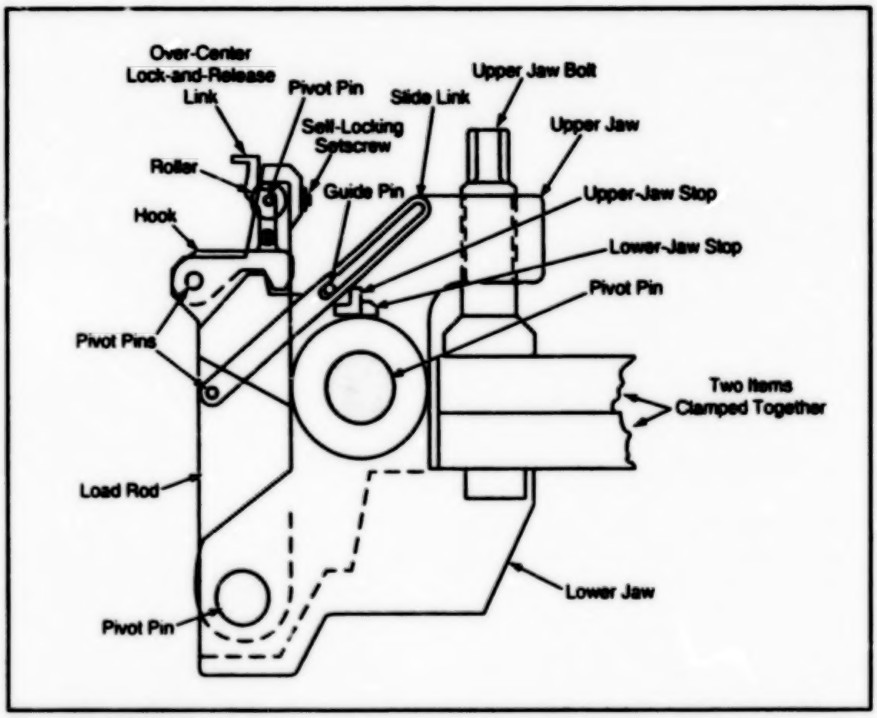

The COSMOWRAP serves the same purpose as does a toggle-action clamp, but is smaller, stiffer, lighter in weight, more easily operable, and more capable.

The term "COSMOWRAP" denotes a compact, stiff, remotely actuatable, lightweight, quick-release clamp that could be substituted for the larger, heavier, and more-difficult-to-use toggle-action clamp now used in the space shuttle orbiter docking system (ODS) to perform contingency separations. In comparison with prior hand-operated devices designed for the same purpose, the COSMOWRAP is smaller and lighter in weight, yet offers greater capabilities. The COSMOWRAP (see figure) contains no spring and requires no pre-flight calibration or maintenance. The COSMOWRAP is expected to perform well, not only in the space-shuttle application for which it was originally designed, but also in terrestrial applications. Because the design of the COSMOWRAP reduces the force needed for installation or removal and provides for release by the action of one hand, the replacement of the ODS toggle-action clamp by the COSMOWRAP can be expected to contribute to crew safety in the United States space program and on the International Space Station.

The toggle action clamp, an adjunct to the ODS, carries a high load and is remotely manually released by use of a tether. As its name implies, it includes a toggle-action mechanism. The mechanism includes an actuating lever. Unfortunately, because of time limits, the design of the toggle-action clamp was not optimized before the clamp was produced. As a result, the toggle-action clamp is heavy as well as very large and cumbersome — a circumstance worsened by need for two such clamps on each spaceflight. The combined assembly length of the toggle-action clamps is >32 in. (>81.3 cm) and each toggle-action clamp weighs 22 lb (a mass of 10 kg). In addition, the operation of the toggle-action clamp is affected by friction in its joints. Because the force needed to operate the toggle-action clamp is greater than that originally expected, a winch tool must be used to perform a release maneuver when the clamp load is high. Moreover, because it is typically necessary to perform pre-flight calibration and checkout, the toggle-action clamp is not only cumbersome but also expensive to use.

The COSMOWRAP is a user-friendly and cost-efficient alternative to the toggle-action clamp and has desirable characteristics not observed in the toggle-action clamp. Among these characteristics are the following:

- The clamping load is significantly higher at release than at installation.
- The COSMOWRAP is capable of remote manual release. Its release load is no more than 25 lb (111 N) [the value required for space missions], although the load on the clamp portion of the COSMOWRAP can approach 10^4 lb (44 kN).
- The clamp can open fully at release to enable separation of previously clamped interfacial components.

Two especially notable features of the COSMOWRAP design are a double-slant interface and an over-center lock-and-release rolling mechanism that provide operational advantages over the toggle-action clamp and enable quick release. Whereas friction in the joints resists oper-

ation of the handle in the toggle-action clamp, the COSMOWRAP design utilizes the friction in the joints in its main load path to reduce the release load. At release, the double-slant interface configuration of the COSMOWRAP enables complete and quick severance of load paths; as a consequence, the components of the COSMOWRAP can be made short and compact, thus contributing to an optimized design characterized by minimum weight and maximum stiffness. Other benefits of the COSMOWRAP design are the following:

- The over-center lock-and-release rolling mechanism enables the COSMOWRAP to lock itself under load.
- The roller mechanism in the COSMOWRAP is not only less adversely affected by friction than is the corresponding mechanism in the toggle-action clamp; in addition, the COSMOWRAP mechanism includes a setscrew that enables the precise adjustment of the release load.
- A slide link makes one-hand operation possible.

Although high-strength-steel components are included in the COSMOWRAP, it could be possible to make some components from aluminum, depending on the magnitude of the load anticipated for the intended application. The required slope of the slant interfaces depends on the finish of interface-bearing surfaces. Once a surface finish and coating have been specified and the corresponding ranges of friction are known, the required slope can be easily determined and verified by simple tests.

Ease of use, a weight-and-space-saving design, and one-handed operation make the COSMOWRAP an attractive addition to the U.S. space program. The COSMOWRAP can be used, for example, to assemble and disassemble a wide variety of highly loaded gasket joints; thus, it can be expected to be suitable for a variety of applications in hazardous environments, not only in outer space but also on Earth (for example, in the repair and construction of pipelines, firefighting, and demolition). The COSMOWRAP can also be used as a quick-release C clamp, jig, or fixture in place of many other lever- and/or toggle-actuated mechanisms.

This work was done by Ted W. Tsai of **Johnson Space Center**.

This invention is owned by NASA, and a patent application has been filed. Inquiries concerning nonexclusive or exclusive license for its commercial development should be addressed to the Patent Counsel, Johnson Space Center, (281) 483-0837. Refer to MSC-22722.

Software for Designing Actively Controlled Structures

One program offers capabilities heretofore available only in separate programs.

John H. Glenn Research Center, Cleveland, Ohio

SMARTCOM is a computer program for the analysis and design of actively controlled "smart" structures. Typically, an actively controlled "smart" structure incorporates piezoelectric sensors and actuators that are used, in conjunction with an electrical control system, to damp vibrations. As is the case for other structures, the analysis and design of actively controlled "smart" structures is often best accomplished with the help of finite-element computer programs. Unfortunately, prior finite-element codes do not offer coupled analyses of the mechanical, electrical, and thermal properties of "smart"-structure materials. Also, they are not directly linked with control software, making it necessary to use separate finite-element and control programs to analyze controlled structures. Furthermore, the programs used heretofore to design "smart" structures do not offer capabilities for optimization or for probabilistic or fuzzy analysis.

In contrast, SMARTCOM offers all of the needed functions and capabilities in one package. SMARTCOM can be used for finite-element modeling of electrical, mechanical, and thermal effects. It includes control algorithms for active damping, algorithms for optimizing the designs of structures, and algorithms for fuzzy and probabilistic modeling of uncertainties.

SMARTCOM comprises several modules that are used, variously, simultaneously or in sequence (see figure). At the present state of development, the modules are the following:

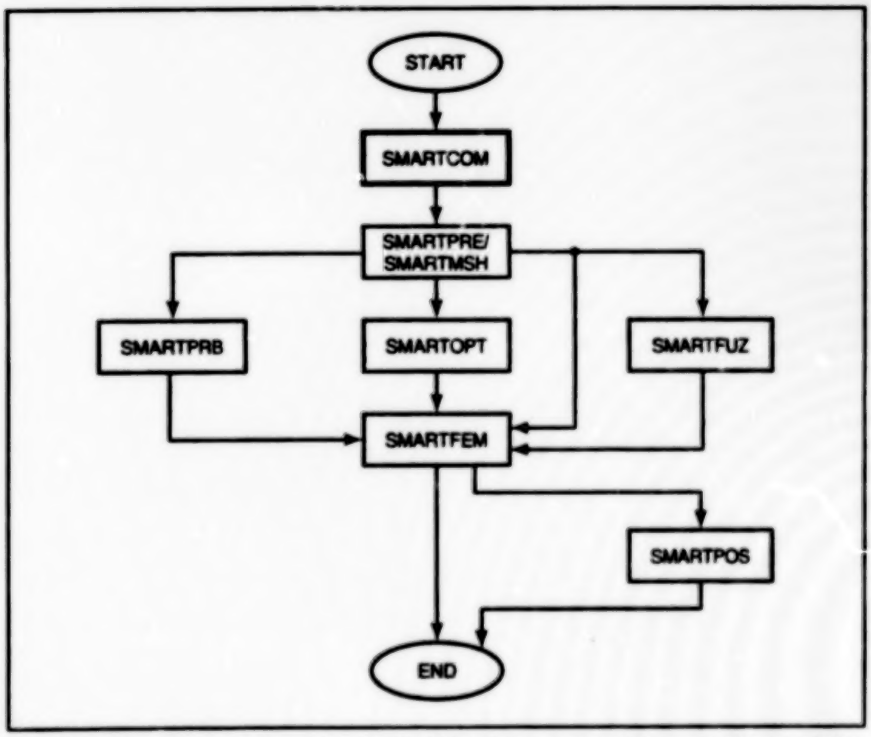

This Data-Flow Diagram shows the relationships among some of the some of the modules of SMARTCOM.

- SMARTCOM (having the same name as that of the overall program) generates a graphical user interface (GUI) and controls the execution of the other modules. The GUI provides easy-to-use dialogues that help the user to specify data, define the problem, specify analysis options, visualize a structure, and visualize the results of the analysis of the structure. The results of the analysis can be displayed in both

textual and graphical forms.

- SMARTPRE preprocesses data for mathematical modeling.
- SMARTMSH generates computational meshes for simple shapes.
- SMARTFEM is a finite-element-analysis code that models mechanical, thermal, and electric fields and is integrated directly with control algorithms.
- SMARTOPT contains optimization algorithms integrated with SMARTFEM.
- SMARTFUZ contains fuzzy modeling algorithms integrated with SMARTFEM.
- SMARTPRB implements probabilistic mathematical models and techniques.
- SMARTPOS postprocesses the results of an analysis for display.

This work was done by Ming S. Hung of Expert System Applications, Inc., for **Glenn Research Center**. *Further information is contained in a TSP [see page 1].*

Inquiries concerning rights for the commercial use of this invention should be addressed to NASA Glenn Research Center, Commercial Technology Office, Attn: Steve Fedor, Mail Stop 4–8, 21000 Brookpark Road, Cleveland, Ohio 44135. Refer to LEW-16810.

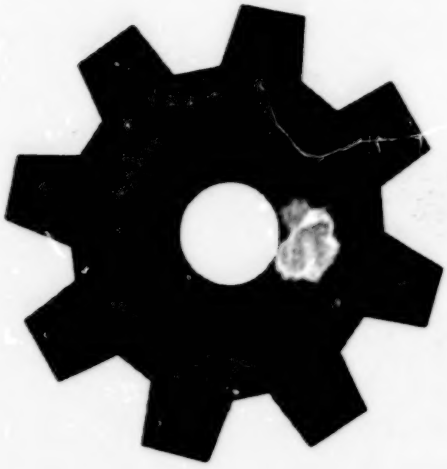

Machinery

Hardware, Techniques, and Processes

BLANK PAGE

Motor Drive for Multiple Horizontally Rotating Bioreactors

Bioreactors can be installed and removed easily.

Lyndon B. Johnson Space Center, Houston, Texas

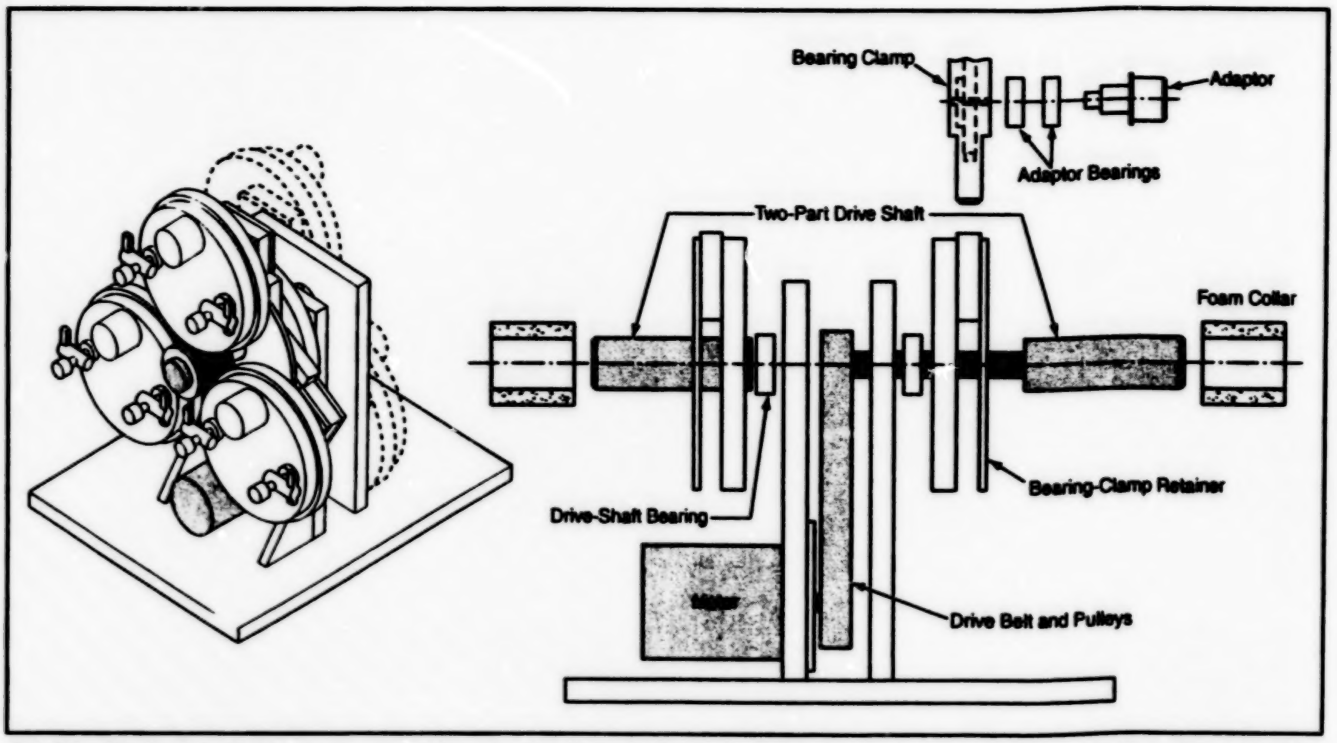

This Drive Mechanism rotates as many as six bioreactor chambers simultaneously. A chamber can be removed during operation, without disturbing the rotation of the other chambers.

The figure depicts a mechanism that is capable of simultaneously rotating as many as six disposable bioreactor chambers about horizontal axes. The particular bioreactor chambers for which this mechanism is designed are high-aspect-ratio vessels (HARVs), which are round cylindrical vessels developed by NASA.

The source of motion is a 24-Vdc geared electric motor with an output shaft speed of 300 rpm in the absence of a load. By means of a toothed drive belt and pulleys, rotation is coupled from the geared-motor output shaft to a drive shaft, which is located centrally relative to the axes of rotation of the bioreactor chambers. The sizes of the pulleys and gear belt can be changed to obtain different speeds of rotation.

Each bioreactor chamber is mounted on an adaptor equipped with bearings that allow free rotation about a horizontal axis. The bearings, in turn, are clamped onto a stationary retainer. A foam collar on each end of the drive shaft makes contact with the outside diameters of the bioreactor chambers, acting as a frictional coupling to transfer rotation of the drive shaft to the bioreactor chambers. The compressibility of the collar accommodates variations in the diameters of the chambers. By loosening the bearing clamp of any given reactor chamber, one can remove that chamber without stopping the rotation of the other chambers.

This work was done by Eric D. Johnston and Mitchell Litt of the University of Pennsylvania for **Johnson Space Center.** *Further information is contained in a TSP* *[see page 1].*

MSC-22860

BLANK PAGE

Mathematics and Information Sciences

Hardware, Techniques, and Processes

BLANK PAGE

Maximum-Likelihood Template Matching

This algorithm features a robust measure of matching and an efficient search technique.

NASA's Jet Propulsion Laboratory, Pasadena, California

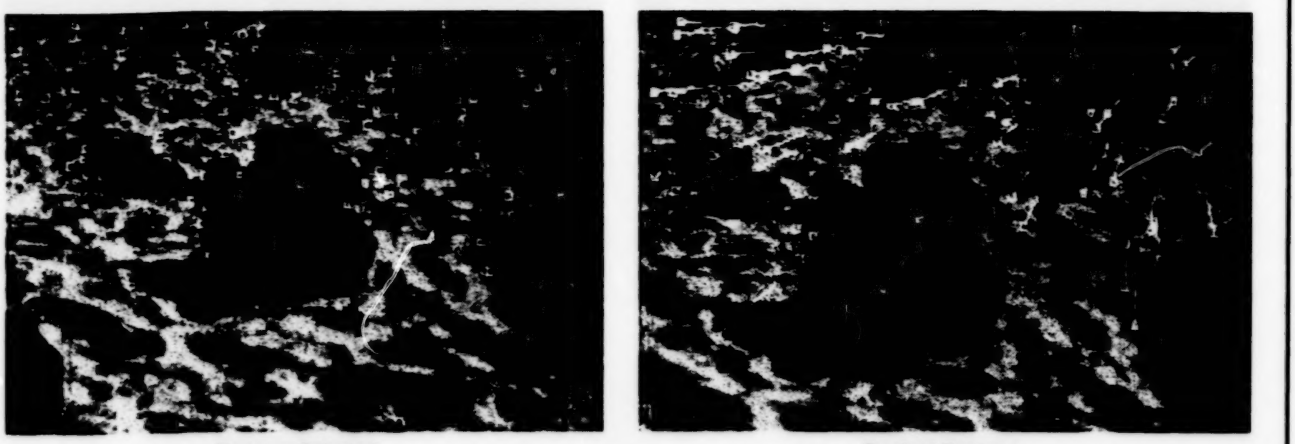

In an Image of Rocky Terrain, 100 7-by-7-pixel feature templates were selected as having the lowest uncertainty for tracking. Tracking was then performed in an image acquired after the camera had undergone forward motion. Seventy-two features survived to be tracked after pruning by use of uncertainty and probability-of-failure measures. No false positives remained among the tracked features.

An improved algorithm for detecting gray-scale and binary templates in digitized images has been devised. The greatest difference between this algorithm and prior template-detecting algorithms stems from the measure used to determine the quality or degree of match between a template and given portion of an image. This measure is based on a maximum-likelihood formulation of the template-matching problem; this measure, and the matching performance obtained by use of it, are more robust than are those of prior template-matching algorithms, most of which utilize a sum-of-squared-differences measure. Other functions that the algorithm performs along with template matching include subpixel localization, estimation of uncertainty, and optimal selection of features. This algorithm is expected to be useful for detecting templates in digital images in a variety of applications, including recognition of objects, ranging by use of stereoscopic images, and tracking of moving objects or features. (For the purpose of tracking, features or objects recognized in an initial image could be used as templates for matching in subsequent images of the same scene.)

For the sake of computational simplicity, the present version of the algorithm involves two-dimensional edge and intensity templates, the pose space of which is restricted to translations in the image plane; however, it is possible, in principle, to extend the algorithm to more complex cases. The basic image-matching technique used in the algorithm utilizes a prior maximum-likelihood formulation of edge template matching that has been extended to include matching of gray-scale templates. In this formulation, one generates a function that assigns a likelihood to each of the possible positions of a template. In an application in which a single instance of the template appears in the image, (e.g., tracking or stereoscopy), one accepts the template position with the highest likelihood if the matching uncertainty is below a specified threshold. In other recognition applications, one accepts all template positions with likelihoods greater than some threshold value.

The search for the template position(s) is performed according a variant of a multiresolution technique that makes it unnecessary to consider all possible template positions explicitly, yet makes it possible to find the best template position(s) in a discretized search space. In this technique, the space of model positions is divided into rectilinear cells and the cells are tested to determine which (if any) contain positions that satisfy a likelihood-based acceptance criterion. The cells that pass the test are divided into subcells, which are examined recursively, and the rest are pruned.

Inasmuch as the likelihood function measures the probability that each position is an instance of the template, error and uncertainty cause the likelihood-function peak that corresponds to that position to be spread over some volume of the pose space. Integration of the likelihood function under the peak yields an improved measure of the quality of the peak as a location of the template. Subpixel localization and estimation of uncertainty are performed by fitting the likelihood surface with a parameterized function at the locations of the peaks. In a stereoscopic or tracking application, the probability of failure to detect the correct position of the template is estimated in a procedure that includes a comparison of the integral of the likelihood under the most likely peak to the integral of the likelihood in the remainder of the pose space.

The foregoing techniques used for matching templates can also be adapted to the optimal selection of features for tracking. This involves estimation of the uncertainty of matching each possible feature with a region of the image in which it might lie. The features at the locations with the lowest uncertainty values are selected as the optimal features for tracking (see figure).

This work was done by Clark F. Olson of Caltech for **NASA's Jet Propulsion Laboratory**. *Further information is contained in a TSP [see page 1].*

NPO-21026

Fast Algorithms and Circuits for Quantum Wavelet Transforms

These theoretical building blocks could be used to implement a variety of quantum algorithms.

NASA's Jet Propulsion Laboratory, Pasadena, California

Fast algorithms and the first complete and efficient circuits for implementing two quantum wavelet transforms have been developed in theory. The significance of this development within the overall development of quantum computing is the following: In principle, the algorithms and circuits constitute instructions for implementing the transforms by use of primitive quantum gates; the circuits in this case are analogous to circuit-diagram-level descriptions of classical electronic circuits that perform logic functions.

Quantum wavelet transforms are fundamental computational operations that can be incorporated into many different quantum algorithms. Such transforms could be useful for optical quantum compression of data and for quantum-enhanced image processing. They may even be useful for estimating quantum states. The two wavelet transforms of interest here are the quantum Haar and the quantum Daubechies $D^{(4)}$ transforms. The approach taken in the development of algorithms and circuits to implement these transforms involved factorization of the classical operators for these transforms into direct sums, direct products, and inner products of unitary matrices to enable efficient quantum implementation.

A particular class of unitary matrices — permutation matrices — play a pivotal role in this factorization. Permutation matrices arise not only in quantum wavelet transforms but also in quantum Fourier transforms and in many classical computations that involve unitary transforms for processing of signals and images. Computational operations that can be performed easily and inexpensively following a classical approach cannot always be performed this way following a quantum approach, and vice versa. The computational cost of permutation matrices is negligible in the classical approach because the matrices can be avoided explicitly, whereas in the quantum approach, permutation operations must be performed explicitly and hence the cost of these operations must be included in the full measure of the complexity and thus the cost of the affected quantum wavelet transforms.

One of the quantum circuits that were developed, denoted the "qubit swap gate," implements a fundamental permutation matrix denoted "Π_4." One can assemble qubit swap gates to implement other fundamental permutation matrices; namely, the perfect-shuffle matrix (Π_{2^n}) and the bit-reversal matrix (P_{2^n}). For quantum computing, the perfect-shuffle and bit-reversal matrices can be characterized directly in terms of their effects on the ordering of qubits. One can assemble building blocks of circuits for these and other matrices to implement the quantum Haar, Daubechies $D^{(4)}$, and wavelet transforms (see figure).

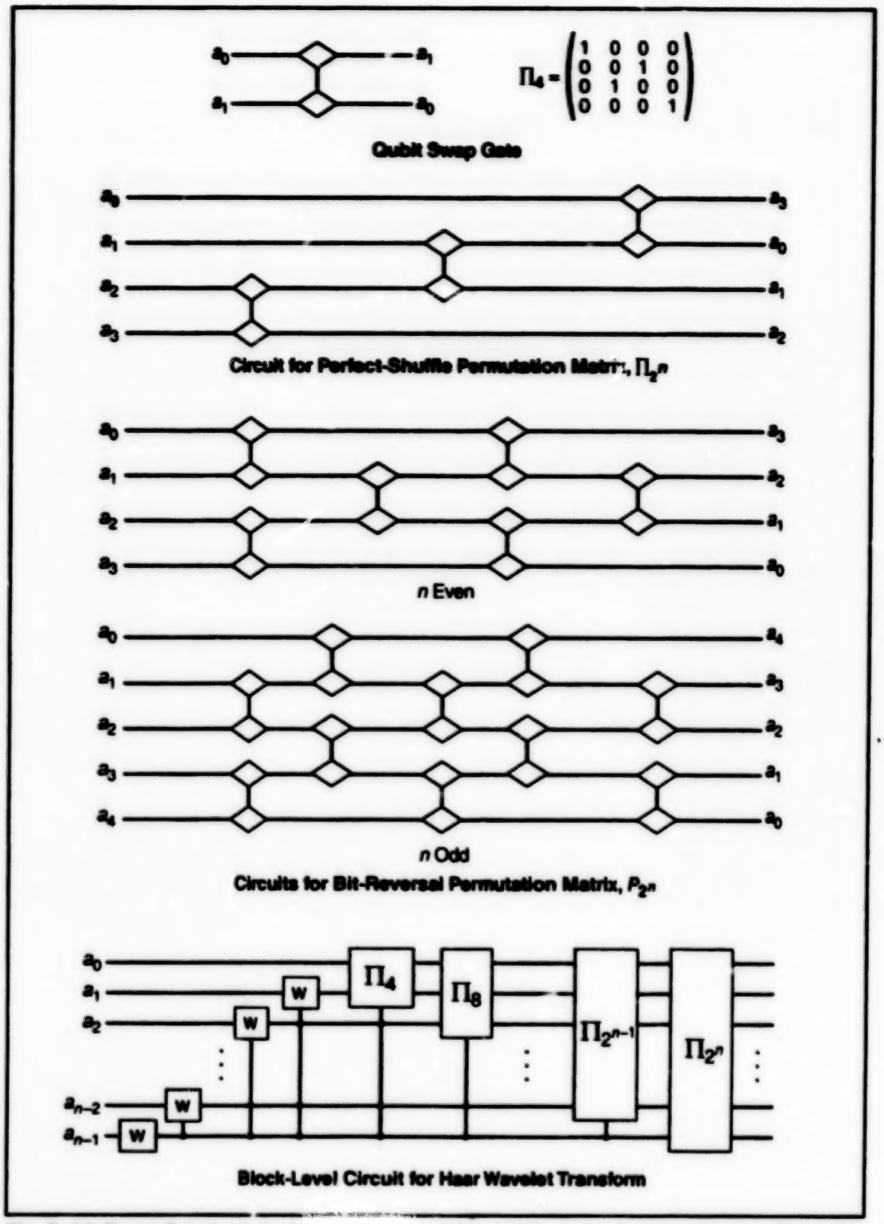

The Qubit Swap Gate implements the Π_4 permutation matrix. A circuit composed of multiple qubit swap gates can implement other fundamental permutation matrices.

The present algorithms and circuits have been validated through extensive simulation. Prior to this development, it had been demonstrated that basic quantum gates can be implemented experimentally by use of nuclear magnetic resonance spectroscopy, cavity quantum electrodynamics, and ion traps. At the time of reporting the information for this article, no one had yet demonstrated that such gates can be integrated together into large-scale quantum circuits; however, efforts to do so were under way at NASA's Jet Propulsion Laboratory.

This work was done by Amir Fijany and Colin Williams of Caltech for **NASA's Jet Propulsion Laboratory**. *Further information is contained in a TSP [see page 1].*
NPO-20747

END

09-10-02